crystals

MDPI

Review

Heterometallic Complexes Containing the Ni^{II}-Ln^{III}-Ni^{II} Moiety—Structures and Magnetic Properties

Catherine P. Raptopoulou

Institute of Nanoscience and Nanotechnology, NCSR "Demokritos", Aghia Paraskevi, 15310 Athens, Greece; c.raptopoulou@inn.demokritos.gr; Tel.: +30-210-650-3346

Received: 19 November 2020; Accepted: 4 December 2020; Published: 8 December 2020

Abstract: This review summarizes the structural characteristics and magnetic properties of trinuclear complexes containing the Ni^{II}-Ln^{III}-Ni^{II} moiety and also oligonuclear complexes and coordination polymers containing the same trinuclear moiety. The ligands used are mainly polydentate Schiff base ligands and reduced Schiff base ligands and, in some cases, oximato, β-diketonato, pyridyl ketone ligands and others. The compounds reported are restricted to those containing one, two and three oxygen atoms as bridges between the metal ions; examples of carboxylato and oximato bridging are also included due to structural similarity. The magnetic properties of the complexes range from ferro- to antiferromagnetic depending on the nature of the lanthanide ion.

Keywords: heterometallic complexes; trinuclear moiety; nickel(II); lanthanide(III) ions; crystal structures; magnetic properties

1. Introduction

The field of Molecular Magnetism emerged as an interdisciplinary field of research between chemists willing to understand the experimental techniques and theoretical tools needed to explain the magnetic properties of coordination compounds and physicists willing to comprehend the molecular structures and intra/intermolecular interactions responsible for the magnetic properties of the above solids. Coordination compounds of various nuclearities and dimensionalities have been the experimental objects for magnetic properties studies and classes of materials with specific properties have been reported, for example Single-Molecule Magnets (SMMs), Single-Ion Magnets (SIMs) and Single-Chain Magnets (SCMs). SMMs can be considered as single molecules behaving like the 'magnetic domains' of bulk magnets and each molecule can be magnetized and retaining its magnetization upon removal of the external magnetic field. Experimentally this can be detected by the presence of out-of-phase signals in ac magnetic susceptibility studies and it was reported for the first time for the 'archetype SMM' compound $[Mn_{12}O_{12}(CH_3COO)_{16}(H_2O)_4]\cdot 2CH_3COOH\cdot 4H_2O$, known as $[Mn_{12}]$ [1]. The complex consists of a cubane unit of four Mn^{IV} ions surrounded by a ring of eight Mn^{III} ions resulting in a ground state of spin $S = 10$ compatible with the alignment of all Mn^{III} spins up and all Mn^{IV} spins down [2,3]. Another well studied SMM in the beginning of Molecular Magnetism was $[Fe_8O_2(OH)_{12}(tacn)_6Br_7(H_2O)]Br\cdot 8H_2O$ (tacn = 1,4,7-triazacyclononane), known as $[Fe_8]$, with ground spin state $S = 10$ corresponding to six Fe^{III} spins up and two Fe^{III} spins down [4,5]. The term SMM is used for oligo/polynuclear coordination clusters, whereas the term SIM was established for mononuclear complexes whose magnetic properties are governed by a single ion. The first 4f SIM is a Tb^{III} double-decker phthalocyanine complex reported in 2003 [6] and the first 3d SIM is a linear Fe^{I} complex reported in 2013 [7]. SCMs are ferromagnetic chains that do not

interact magnetically with each other and were first realized in a 1D coordination polymer consisting of $Co(hfac)_2$ and a radical ligand which behaves as 1D ferrimagnet [8].

Fundamental in Molecular Magnetism is the presence of unpaired electrons that must be interact with other unpaired electrons occupying p, d and f magnetic orbitals, originating from organic radical ions, transition metal ions and lanthanide metal ions, respectively. The versatile chemistry of transition metal ions offers structural variety of coordination compounds with a wide range of unusual magnetic properties, related to the various oxidation states and electronic properties of the cations, splitting of the d orbitals upon complexation and variability of coordination geometries. Lanthanides display unique magnetic properties because of the contributions from the spin and orbit motion of the electrons and magnetocrystalline anisotropy (single-ion anisotropy) associated with crystal-field and spin-orbit coupling. The chemistry of lanthanides differs significantly from that of transition metals due to the shielding of the f electrons by the external $5s^2$ and $5p^6$ shells. As a consequence, the f electrons do not contribute to bonding upon coordination and therefore, the interactions between the f electrons and ligand orbitals are very weak and only strong electronegative atoms are able to bind to a lanthanide ion. Another important aspect is that all the 4f ions are able to form complexes without substantial geometrical differences in the geometrical environment, which is extremely helpful in molecular magnetism in order to study complexes of different electronic structures albeit of similar geometrical characteristics. The interest on heterometallic transition metal (TM) and lanthanide (Ln) ions complexes is based on the possibility to achieve high spin ground states along with large single-ion anisotropy that can potentially provide SMM behavior.

The synthetic approaches to heterometallic TM/Ln complexes involve two strategies, the 'metal complexes as ligands' and the 'one-pot.' The first, uses mono- or di-nuclear complexes of TM (metalloligands) with uncoordinated O-donor sites that can react with the Ln ions. The second, requires a mixture of TM and Ln salts and organic ligands containing distinct coordination compartments (pockets) for the preferential binding of the metal ions. The HSAB model plays an important role in this approach because Ln ions are hard Lewis acids and prefer hard O-sites whereas TM are soft and borderline Lewis acids and prefer N-atoms or purely soft bases (i.e., S-atoms) [9]. For example, the mononuclear octahedral complex $[Ni(mpko)_2(mpkoH)]$ (mpkoH = methyl 2-pyridyl ketone oxime) was used as metalloligand according to the 'metal complexes as ligands' strategy to obtain dinuclear $[NiLn(NO_3)_3(mpko)_2(mpkoH)]$, trinuclear $[Ni_2Ln(mpko)_6](NO_3)$ and tetranuclear complexes $[Ni_2Ln_2(NO_3)_4(mpko)_6]$ (Ln = Gd-Er) [10,11]. Among the ligands containing coordination compartments for the 'one-pot' strategy, Schiff bases have been widely used because they can be easily prepared and modified with the desired substituents and functional groups. For example, the heterometallic complex $[CuTbL(hfac)_2]_2$ (H_3L the Schiff base ligand 1-(2-hydroxybenzamido)-2-(2-hydroxy-3-methoxy-benzylidenamino)ethane, Hhfac = hexafluoroacetylacetone) was the first SMM containing Ln ions [12]. Soon after the observation of ferromagnetic interactions in a Cu_2Gd complex [13], synthetic strategies were developed for the designed synthesis of dinuclear TM/Ln complexes in order to investigate the nature and magnitude of the magnetic interactions between the metal ions [14,15]. Trinuclear TM_2Ln complexes have been also reported and some have been found to display SMM properties [16].

The present review emphasizes on the reported trinuclear Ni-Ln-Ni complexes, oligonuclear complexes and coordination polymers containing the Ni-Ln-Ni moiety, their structural characteristics and magnetic behavior which ranges from ferro-to antiferromagnetic depending on the nature of the lanthanide ion. The ligands used are mainly Schiff bases based on salicylaldehyde, o-vanillin and tripodal, dipodal aliphatic and aromatic amines; few examples are reported with diketonato or other type of ligands.

2. Discussion

The review describes the trinuclear complexes that contain the Ni^{II}-Ln^{III}-Ni^{II} moiety classified according to the type of organic ligands used in Section 2.1. The oligonuclear complexes and the

coordination polymers that contain the Ni^{II}-Ln^{III}-Ni^{II} moiety are presented in Sections 2.2 and 2.3. respectively. The structural characteristics of the complexes, magnetic exchange parameters, energy barriers and pre-exponential factors of the reported complexes are given in Tables 1–3.

Table 1. Structural characteristics of the crystallographically studied Ni_2Ln complexes.

Complex	Ni^{II} Coordination Mode	Ln^{III} Coordination Mode	Ni-Ln-Ni Angle (°)	Ln^{III}	Ref.
$[(NiL^1)_2Ln](ClO_4)$	N_3O_3	O_{12}	176.2–178.7	La-Er except Pm	[17,18]
$[(NiL^2)_2Ln](NO_3)$	N_3O_3	O_8	139.9–143.8	Eu, Gd, Tb, Dy	[19,20]
$[(NiL^3)_2Ln](NO_3)$	N_3O_3	O_{12}	178.4–178.7	Gd	[21]
$[(NiL^4)_2Ln](NO_3)$	N_3O_3	O_6/O_7	177.1–177.8	Gd, Tb, Dy	[22]
$[(NiL^4)_2Ln](ClO_4)$	N_3O_3	O_6	174.6	Dy	[22]
$[(NiL^5)_2Ln(solv)_x](ClO_4)$ [a]	N_3O_3	$O_6/O_7/O_8$	142.5–157.7	La, Dy, Yb	[23]
$[(NiL^6)_2Ln(MeOH)](NO_3)$	N_4O_2	O_7	139.6–143.9	La, Sm, Tb, Er, Lu	[24,25]
$[(NiL^6)_2Ln(MeOH)](ClO_4)$	N_4O_2	O_7	143.9	Pr	[24]
$[(NiL^7)_2Ln](ClO_4)_2$	N_4O_2	O_8	113.0, 113.3	Gd, Dy	[26]
$[(NiL^8)_2Ln(MeCN)_2](ClO_4)$	N_3O_3	N_2O_6	142.4	Gd	[27]
$[(NiL^8)_2Ln](ClO_4)$	N_3O_3	O_6	176.4	Yb	[27]
$[(NiL^9)_2Ln(solv)_x](ClO_4)$ [b]	N_3O_3	O_6, O_7	165.1–178.8	Y, Ce-Lu except Pm, Yb	[28]
$[(NiL^{10})_2Ln](ClO_4)$	N_3O_3	O_6	180.0	Tb	[29]
$[(NiL^{11})_2Ln](NO_3)$	N_3O_3	O_{12}	179.7–179.9	La, Pr, Gd, Tb	[30,31]
$[\{Ni(HL^{12})_2\}_2Ln(NO_3)](NO_3)_2$	N_2O_4	O_{10}	169.2	La	[32]
$[\{Ni(H_3L^{13})_2\}_2Ln](NO_3)_3$	N_2O_4	O_8	179.3–179.6	Gd, Tb, Dy, Ho	[33]
$[\{Ni(H_3L^{14})_2\}_2Ln(O_2CMe)_2](NO_3)_3$	N_2O_4	O_8	180.0	Gd, Tb	[34]
$[(NiL^{15})_2Ln(NO_3)_2](NO_3)$	N_2O_2	O_{12}	67.8, 67.9	La, Ce	[35]
$[(NiL^{16})_2Ln(NO_3)_2](NO_3)$	N_2O_2	O_{12}	62.1	Ce	[36]
$[(NiL^{17})_2Ln(O_2CMe)_2(MeOH)_2](NO_3)$	N_2O_4	O_{10}	180.0	La, Nd, Ce, Pr	[37,38]
$[(NiL^{18})_2Ln(NO_3)_3]$	N_2O_2	O_{10}	122.5	Ce	[39]
$[\{Ni(L^{19})(H_2O)\}_2Ln(H_2O)](trif)_3$ [c]	N_2O_3	O_9	179.0, 177.2	Gd, Eu	[21,40]
$[\{Ni(H_2L^{20})_2(tren)_2\}_2Ln](NO_3)_3$ [d]	N_5O	O_8	93.0–95.3	Gd, Dy, Er, Lu	[41]
$[\{Ni(L^{21})_3\}_2Ln(L^{21})]$	N_3O_3	NO_7	129.6	La	[42]
$[\{Ni(L^{22})_{1.5}\}_2Ln(OH)]$	N_3O_3	O_9	180.0	Eu, Gd, Tb	[43]
$(Me_4N)[\{Ni(L^{23})_3\}_2Ln(L^{23})_2]$	N_6	N_2O_8	141.3–142.5	La, Ce, Pr, Nd, Sm	[44]
$(Et_4N)_2[\{Ni(L^{23})_3\}_2Ln(dcnm)_2](ClO_4)_2$ [e]	N_6	N_2O_8	133.1, 133.2	La, Ce	[44]
$[(NiL^{24})_2Ln(NO_3)_2(MeOH)_4](NO_3)$	O_6	N_2O_8	180.0	La, Ce, Pr, Nd, Sm, Eu	[45]
$[(NiL^{24})_2Ln(NO_3)_2(H_2O)_2(MeOH)_2](NO_3)$	O_6	N_2O_8	177.6–177.8	Sm, Eu, Gd	[45]
$[(NiL^{24})_2Ln(NO_3)_3(MeOH)_4]$	O_6	N_2O_8	172.6–172.9	Gd, Tb, Dy	[45]
$[(NiL^{24})_2Ln(NO_3)_2(H_2O)(MeOH)_3](NO_3)$	O_6	N_2O_8	179.4–179.5	Ho, Er, Tm, Yb, Lu	[45]
$[(NiL^{25})_2Ln(O_2CMe)_3(MeOH)_x]$ [f]	O_6	N_2O_7,N_2O_8	178.0–178.2	Ce, Gd	[46]
$[(NiL^{25})_2Ln(O_2CPh)_3(solv)_x]$ [g]	O_6	N_2O_8	176.6	Gd	[46]
$[(NiL^{26})_2Ln(O_2CMe)_3(MeOH)_2]$	O_4S_2	N_2O_8	176.9	Pr	[47]
$[\{Ni(piv)_3(bpy)\}_2Ln(NO_3)]$ [h]	N_2O_4	O_8	152.9, 153.3	Sm, Gd	[48]
$[\{Ni(piv)_3(Hpiv)(MeCN)\}_2Ln(NO_3)]$	NO_5	O_8	144.0	Sm	[48]
$[\{Ni(L^{27})_3\}_2Ln](NO_3)$	N_3O_3	O_6	180.0	Tb	[10,11]
$[(Ni(HL^{28})_3\}_2Ln](NO_3)$	N_3O_3	O_6	180.0	Tb	[49]
$[Ni_2(L^{29\prime})_3(L^{29\prime\prime})Ln(NO_3)(H_2O)](ClO_4)_2$	N_3O_3	N_2O_6	54.2, 54.4	Gd, Tb	[50,51]
$[Ni_2(L^{29\prime})_4Ln(NO_3)(H_2O)][Ln(NO_3)_5](ClO_4)_2$	N_3O_3	N_2O_6	53.7	Tb, Dy, Y	[50,51]
$[\{\{(NiL^{30}(H_2O))(N(CN)_2)\}_2Ln\}_2(\mu\text{-}NO_3)](OH)$	N_3O_3	O_9, O_{10}	175.7	Pr	[52]

Table 1. *Cont.*

Complex	Ni^{II} Coordination Mode	Ln^{III} Coordination Mode	Ni-Ln-Ni Angle (°)	Ln^{III}	Ref.
$[\{Ni_2(L^{24})Ln(H_2O)_4\}_2(C_2O_4)_3]$	O_6	N_2O_8	178.6	Gd	[53]
$[\{Ni(L^{19})_2\}_2Ln(H_2O)Fe(CN)_6]_2$	N_3O_2	O_9	179.1	Dy	[54]
$[(Ni(L^{19})_2\}_2Ln(H_2O)Cr(CN)_6]_2$	N_3O_2	O_9	177.6–178.5	Y, Gd, Tb, Dy	[55]
$[(Ni(L^{19})_2\}_2Ln(H_2O)Fe(CN)_6]_2$	N_3O_2	O_9	177.8–179.3	Y, Gd, Tb	[55]
$[(Ni(L^{19})_2\}_2Ln(H_2O)Co(CN)_6]_2$	N_3O_2	O_9	177.8	Dy	[55]
$[(Ni(L^{19})_2\}_2Ln(H_2O)W(CN)_8]_2$	N_3O_2	O_9	175.2/177.1 [i]	Tb, Dy, Y	[56]
$[(Ni(L^{19})_2\}_2Ln(H_2O)Co(CN)_6]_2$	N_3O_2	O_9	177.6	Tb	[56]
$[\{(NiL^{31})_2Ln(NO_3)_3\}pyz]_n$	N_3O_3	O_9	149.6, 153.5	Dy	[57]
$[\{(NiL^{24})_2Ln(H_2O)_4(oxy\text{-}bbz)\}(NO_3)]_n$	O_6	N_2O_8	178.8	Dy	[58]
$[\{[Ni(L^{32})_{1.5}]_2Ln(H_2O)_5\}(CF_3SO_3)]_n$	N_6	O_7	96.7	Tb	[59]
$[\{[Ni(L^{32})_{1.5})]_2Ln(H_2O)_4(NO_3)]_n$	N_6	O_8	99.2, 99.3	Gd, Tb	[59]
$[\{[Ni(L^{33})_{1.5}]_2Ln(H_2O)_5\}(NO_3)]_n$	N_6	O_7	99.8	Tb	[60]
$[\{[Ni(L^{33})_{1.5}]_2Ln(H_2O)_6\}(CF_3SO_3)]_n$	N_6	O_8	72.8, 73.1	Tb, Dy	[60]
$[\{(Ni(H_2L^{34}))_2Ln(H_2O)_3\}(ClO_4)_3]_n$	N_4	O_9	179.2–179.4	Pr, Sm, Gd	[61]
$[\{(Ni(L^{35})_{1.5})_2Ln(HL^{35})(dmf)_4\}(ClO_4)_4]_n$	N_4O_2	O_8	111.5, 111.9	Gd, Tb	[62]
$[\{(Ni(L^{35})_2)_2Ln(dmf)_4\}(ClO_4)_3]_n$	N_4O_2	O_8	115.1	Dy	[62]
$[\{Ni(L^{36})_{1.5}\}_2Ln(dpds)_2(H_2O)_4]_n$	N_2O_4	O_9	145.7	Eu	[63]
$[\{Ni(L^{37})_{2.5}(N_3)(H_2O)\}_2Ln(H_2O)]_n$	N_3O_3	O_9	84.9–131.8	Gd, Pr, Nd	[64,65]

[a] x = 2 H_2O/$(MeOH)_{0.5}$/$(EtOH)_{0.5}$ in Ni_2La, x = 2 H_2O/MeOH in Ni_2Dy, x = 1, H_2O in Ni_2Yb; [b] x = 1 H_2O in Ni_2Sm/Ni_2Eu/Ni_2Tb x = 0 in all other complexes; [c] trif = $CF_3SO_3^-$; [d] tren = tris(2-aminoethyl)amine; [e] dcnm = dicyanonitrosomethanide; [f] x = 2 or 3; [g] x = 2 MeOH in Ni_2Gd, x = 2 MeOH/H_2O in Ni_2Ce; [h] Hpiv = pivalic acid, bpy = 2,2′-bipyridine; [i] average values for two crystallographically independent molecules.

Table 2. Magnetic exchange parameters of the trinuclear Ni_2Ln complexes.

Complex	J_{NiLn} (cm^{-1})	J_{NiNi} (cm^{-1})	g_{Ni}/g_{Ln}	D (cm^{-1})	Ref
$[(NiL^1)_2Gd](ClO_4)$	+0.375		2.04		[17]
$[(NiL^2)_2Gd(NO_3)]$	+0.19		2.24	+2.1	[19,20]
$[(NiL^3)_2Gd](NO_3)$	0.91		1.98	4.5	[21]
$[(NiL^4)_2Gd](NO_3)$ [a]	0.64		2.04		[22]
$[(NiL^7)_2Gd)](ClO_4)$	1.02		2.01		[26]
$[(NiL^9)_2Y(solv)_x](ClO_4)$ [b]		−0.294	2.09	1.933	[28]
$[(NiL^9)_2Lu(solv)_x](ClO_4)$ [c]		−0.129	2.18	2.838	[28]
$[(NiL^9)_2Gd(solv)_x](ClO_4)$ [d]	−0.009	−0.377	2.102/1.974		[28]
$[(NiL^{11}{}_3)_2Gd](NO_3)$	+0.54		2.01/2.01		[30,31]
$[(NiL^{11}{}_3)_2La](NO_3)$		+0.46	2.245	+4.91	[30,31]
$[\{Ni(HL^{12})_2\}_2La(NO_3)](NO_3)_2$		−0.978	2.177	3.133	[32]
$[\{Ni(H_3L^{13})_2\}_2Gd](NO_3)_3$	+0.67		2.117	4.92	[33]
$[\{Ni(H_3L^{14})_2\}_2Sm(O_2CMe)_2](NO_3)_3$ [e]		−0.37	1.97		[34]
$[\{Ni(H_3L^{14})_2\}_2Gd(O_2CMe)_2](NO_3)_3$	+0.42		1.98/1.98	+2.95	[34]
$[(NiL^{17})_2La(O_2CMe)_2(MeOH)_2](NO_3)$		−0.75	2.18		[37,38]
$[(NiL^{17})_2Ce(O_2CMe)_2(MeOH)_2](NO_3)$		−1.1	2.23		[37,38]
$[(NiL^{17})_2Pr(O_2CMe)_2(MeOH)_2](NO_3)$		−1.3	2.15		[37,38]
$[\{NiL^{19}(H_2O)\}_2Gd(H_2O)](trif)_3$ [f]	4.8		2.03	0.03	[21,40]
$[\{Ni(H_2L^{20})(tren)_2\}_2Gd](NO_3)_3$	−0.083		2.03		[41]
$[\{Ni(H_2L^{20})(tren)_2\}_2Lu](NO_3)_3$			2.19	3.2	[41]

Table 2. *Cont.*

Complex	J_{NiLn} (cm^{-1})	J_{NiNi} (cm^{-1})	g_{Ni}/g_{Ln}	D (cm^{-1})	Ref
$[(NiL^{24})_2La(NO_3)_3(H_2O)_4]$		−0.63	2.22		[45]
$[(NiL^{24})_2Lu(NO_3)_3(H_2O)_4]$		−0.65	2.17		[45]
$[(NiL^{24})_2Gd(NO_3)_3(H_2O)_4]$ [g]	+0.79		2.20/2.02		[45]
$[\{Ni(piv)_3(bpy)\}_2Gd(NO_3)]$ [h]	+0.105	−0.70	2.015/2.0		[48]
$[\{Ni(piv)_3(Hpiv)(MeCN)\}_2Gd(NO_3)]$ [i]	0.44	−2.25	2.0/2.0		[48]
$[\{Ni(piv)_3(Hpiv)(MeCN)\}_2La(NO_3)]$ [j]		−1.0	2.24		[48]
$[Ni_2(L^{29\prime})_3(L^{29\prime\prime})Gd(NO_3)(H_2O)](ClO_4)_2$ [k]	+1.03		2.246		[50,51]
$[Ni_2(L^{29\prime})_4Y(NO_3)(H_2O)][Ln(NO_3)_5](ClO_4)_2$ [l]		0	2.15		[50,51]

[a] $zJ' = 0.0009$ cm^{-1}; [b] $E/D = 0.154$ cm^{-1}; [c] $E/D = 0.468$ cm^{-1}; [d TIP] = 0.003 cm^3Kmol^{-1}; [e] TIP = 0.001 cm^3mol^{-1}; [f] $j_{NiGd} = 0.05(2)$ cm^{-1}; [g] $J' = -0.64$ cm^{-1}; [h] tip = 0.0001; [i] including molar content of the $S = 1$ impurity is 5.5%; [j] $zJ' = +0.9(1)$ cm^{-1}, tip = $2.4(9) \times 10^{-4}$; [k] $J' = +0.9(2)$ cm^{-1}; [l] $J' = +8.0(2)$ cm^{-1}.

Table 3. Complexes containing the Ni^{II}-Ln^{III}-Ln^{II} moiety that behave as Single-Molecule Magnets (SMMs).

Complex	U (K)	τ_0 (s)	Ref.
$[(NiL^1)_2Dy](ClO_4)$ [a]	10.8	2.3×10^{-5}	[17]
$[(NiL^4)_2Dy](NO_3)$ [b]	14.17	1.09×10^{-6}	[22]
$[(NiL^4)_2Dy](ClO_4)$ [b]	11.13	6.72×10^{-6}	[22]
$[\{Ni(L^{19})_2\}_2Dy(H_2O)Fe(CN)_6]_2$ [b]	25.0	1.6×10^{-7}	[54]
$[(Ni(L^{19})_2\}_2Tb(H_2O)Cr(CN)_6]_2$ [b]	21.9	4.71×10^{-8}	[55]
$[(Ni(L^{19})_2\}_2Dy(H_2O)Cr(CN)_6]_2$ [b]	38.9	4.89×10^{-9}	[55]
$[(Ni(L^{19})_2\}_2Dy(H_2O)Cr(CN)_6]_2 \cdot 2PPPO$ [c]	37.2	6.44×10^{-9}	[55]
$[(Ni(L^{19})_2\}_2Tb(H_2O)Fe(CN)_6]_2$ [b]	29.6	4.52×10^{-10}	[55]
$[(Ni(L^{19})_2\}_2Dy(H_2O)Co(CN)_6]_2$ [b]	24.4	4.94×10^{-7}	[55]
$[(Ni(L^{19})_2\}_2Tb(H_2O)W(CN)_8]_2$ [b]	23.0	2.57×10^{-7}	[56]
$[(Ni(L^{19})_2\}_2Dy(H_2O)W(CN)_8]_2$ [b]	26.4	6.0×10^{-8}	[56]

[a] under 3500 Oe dc field; [b] under zero dc field; [c] PPPO = 4-(3-phenylpropyl)pyridine-1-oxide.

2.1. Trinuclear Ni^{II}-Ln^{III}-Ni^{II} Complexes

2.1.1. Tripodal Polydentate Schiff Base Ligands and Reduced Schiff Base Ligands

A new phosphorus-supported ligand H_3L^1 = (S)P[M(Me)N=CH-C_6H_3-2-OH-3-OMe]$_3$ (Scheme 1), prepared by the condensation of (S)P[M(Me)NH_2]$_3$ and *o*-vanillin, was used to synthesize the trinuclear isomorphous complexes $[(NiL^1)_2Ln](ClO_4)$ (Ln = La-Er, except Pm, **1**–**11**) [17]. The cation consists of three nearly linear metal ions, two terminal Ni^{II} and one Ln^{III} in the center (Figure 1). Each of the terminal Ni^{II} is bound to the three imino nitrogen and the three phenolato oxygen atoms of one $(L^1)^{3-}$, thus describing an in situ formed $[NiL^1]^-$ metalloligand. Two such metalloligands are bound to the central Ln^{III} ion through the phenolato and methoxy oxygen atoms of the two ligands, describing a distorted icosahedral. The Ln-O bond distances show a gradual reduction in accordance with lanthanide contraction. The Ni_2Gd (**7**), Ni_2Dy (**9**) and Ni_2Er (**11**) complexes display ferromagnetic interactions between the metal ions. The magnetic susceptibility measurements of **7** were interpreted by using the spin Hamiltonian $H = -2J(S_{Ni1}S_{Gd} + S_{Gd}S_{Ni2})$ where $S_{Ni1} = S_{Ni2} = 1$ and $S_{Gd} = 7/2$. The best set of parameters obtained using this model is $J/k_B = +0.375$ cm^{-1} and $g = 2.04$. The magnetization measurements of **7** as a function of the field show relatively rapid saturation of the magnetization at high fields and agree with an $S = 11/2$ spin ground state. Ac susceptibility measurements of the Ni_2Dy complex (**9**) as a function of the temperature at different frequencies and also as a function of the frequency at different temperatures under zero and 3500 Oe dc field showed that **9** exhibits slow relaxation of the magnetization and observation of field induced single-molecule magnet behavior. The data were fitted to an Arrhenius law in order to estimate the energy gap of 10.8 K and pre-exponential factor $\tau_0 = 2.3 \times 10^{-5}$ s. The value of 10.8 K is in the range observed for

similar complexes, however the value of τ_0 is much larger than expected suggesting that the quantum pathway of relaxation is only partially suppressed by the applied field of 3500 Oe and hence that the energy gap of the thermally activated relaxation should be higher than 10.8 K. In any case, the magnetic study of **9** suggests SMM behavior generated by the high spin ground state of the complex and the magnetic anisotropy of the Dy^{III} ion. All other complexes behave as simple paramagnetic systems. DFT calculations on the Ni_2Gd (**7**) and Ni_2La (**1**) complexes revealed good agreement between the experimental and computed *J* values, confirmed the ferro- and antiferromagnetic nature of the J_{NiGd} and J_{NiNi} interactions, respectively and gave information on the spin densities of the metal ions and bridging oxygen atoms [18].

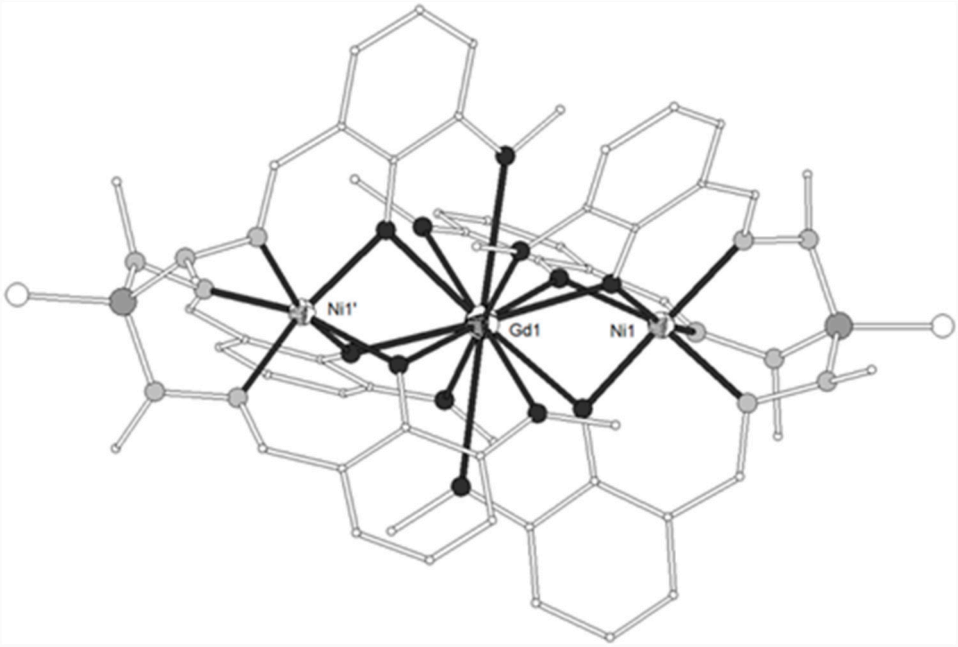

Figure 1. The molecular structure of the cation $[(NiL^1)_2Gd]^+$ in complex **7**. Primed atoms are generated by symmetry: (') = $-x$, y, $1-z$. Color code: Gd large octant, Ni small octant, N light grey, O dark grey, C open small, P grey large, S open large [17].

The tripodal hexadentate Schiff base-phenolate ligand H_3L^2 = 2,2′-((1*E*)-((2-(((*E*)-(2-hydroxybenzylidene)amino)methyl)-2-methylpropane-1,3-diyl)bis(azanylylidene))bis(methanylylid ene))diphenol (Scheme 1) was used to synthesize the neutral trinuclear complexes $[(NiL^2)_2Ln(NO_3)]$ (Ln^{III} = Gd, Eu, Tb, Dy, **12**–**15**) [19,20] which show a Ni-Ln-Ni angle of ca. 140° (Figure 2). All four complexes have similar structures with the two terminal Ni^{II} ions coordinated to the three imino nitrogen and three phenolato oxygen atoms of one $(L^2)^{3-}$. The coordination geometry of each Ni^{II} ion is distorted from a regular octahedron toward a trigonal prism with trigonal twist angle ϕ ~45° (trigonal prism = 0°, octahedron = 60°). The central Ln^{III} ion is bound to the phenolato oxygen atoms of the ligands and to chelate nitrato ligand. All complexes exhibit 3D structures due to intermolecular π-π and CH-π interactions between neighboring molecules. The magnetic data for the Ni_2Gd (**12**) complex are consistent with ferromagnetic coupling between the metal ions giving rise to a ground state with spin S = 11/2. The best-fit parameters to the experimental magnetic susceptibility data of **12** were g = 2.24, J(Ni-Gd) = +0.19 cm^{-1} and D = +2.1 cm^{-1}. A ferromagnetic interaction is also suggested for the Ni_2Tb (**14**) and Ni_2Dy (**15**) complexes.

The complex $[(NiL^3)_2Gd](NO_3)$ (**16**) (H_3L^3 = 6,6′-((1*E*)-((2-(((*E*)-(2-hydroxy-3-methoxybenzylidene) amino)methyl)-2-methylpropane-1,3-diyl)bis(azanylylidene))bis(methanylylid ene))bis(2-methoxyphenol), Scheme 1) contains also two $[NiL^3]^-$ metalloligands bound to a Gd^{III} ion in an almost linear arrangement

(~178°) [21]. The asymmetric unit contains two different cationic entities, the first one possesses two slightly different Ni^{II} environments, while the second one is symmetry-related through the Gd^{III} ion (Supplementary Materials Figure S1). The coordination geometry around each Ni^{II} ion is distorted octahedral with N_3O_3 chromophore. The Gd^{III} ion is coordinated to twelve oxygen atoms, deprotonated phenoxo oxygens and neutral methoxy oxygens. The magnetic susceptibility data were interpreted in terms of the spin Hamiltonian $H = -J_{NiGd}(S_{Ni1}S_{Gd} + S_{Ni2}S_{Gd}) + D\left(S_z^2Ni1 + S_z^2Ni2\right)$ considering two equivalent Ni1-Gd and Ni2-Gd exchange interactions J and identical ZFS terms D. The best-fit parameters are J_{NiGd} = 0.91 cm^{-1}, g = 1.98 and D = 4.5 cm^{-1}. The magnetization measurements at 2 K in the range 0–5 T were satisfactorily simulated with this set of parameters and confirmed an S = 11/2 ground state due to ferromagnetic coupling between the metal ions.

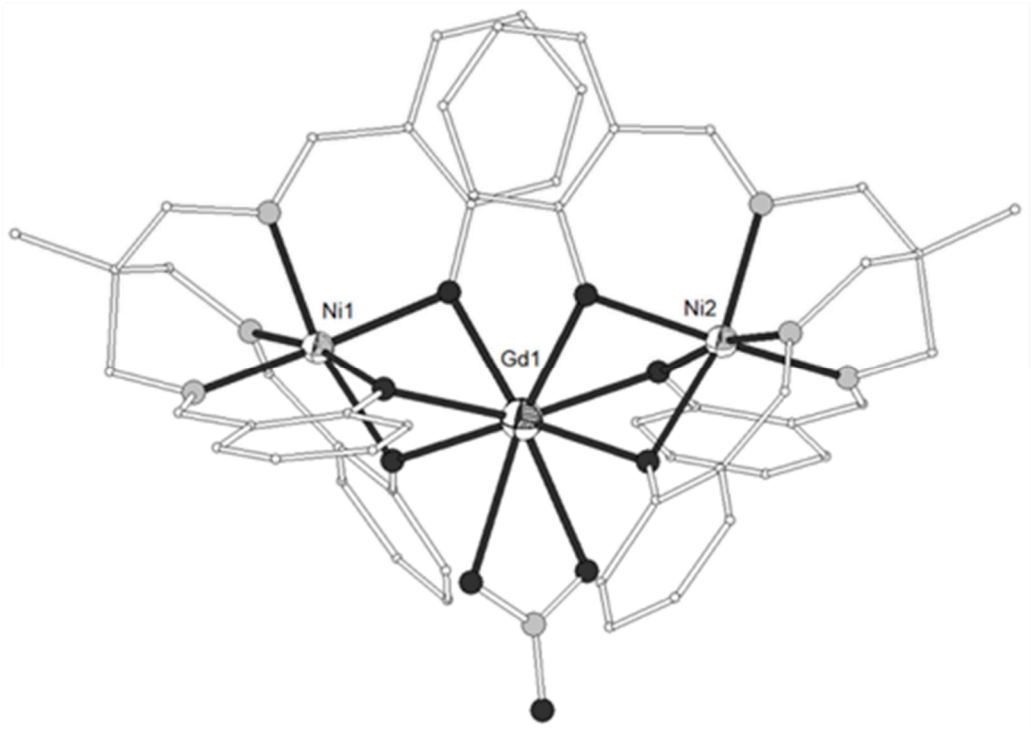

Figure 2. The molecular structure of complex $[(NiL^2)_2Gd(NO_3)]$ (**12**). Color code: Gd large octant, Ni small octant, N light grey, O dark grey, C open small [19].

The tripodal ligand H_3L^4 = 6,6′,6″-((1*E*,1′*E*)-((nitrilotris(ethane-2,1-diyl))tris (azanylylidene)) tris(methanylylidene))tris(2-methoxyphenol) (Scheme 1) gave four heterometallic complexes, $[(NiL^4)_2Ln](NO_3)$ (Ln^{III} = Gd, Tb, Dy, **17**–**19**) and $[(NiL^4)_2Dy](ClO_4)$ (**20**) which contain linear Ni-Ln-Ni moieties (Figure 3) [22]. The Gd^{III} ion exhibits rare seven-coordination to six bridging phenoxo oxygen atoms and one methoxy oxygen atom from one of the $(L^4)^{3-}$ ligands and can be considered as an intermediate between the capped trigonal prism (CTPR-7, C_{2v}) and the capped octahedron (CTPR-7, C_{3v}). The Ln^{III} ions in the remaining three complexes exhibit rare six-coordination which can be described as quasi trigonal antiprism (intermediate between octahedron OC-6, O_h and trigonal prism TPR-6 D_{3h}). The magnetic susceptibility measurements of **17** were interpreted by using the spin Hamiltonian $\hat{H} = -2J\hat{S}_{Gd1}\left(\hat{S}_{Ni1} + \hat{S}_{Ni2}\right)$ and gave the best-fit parameters g = 2.04, J = 0.64 cm^{-1} and zJ' = 0.009 cm^{-1} ($R = 6.99 \times 10^{-3}$). The magnetization at 1.8 K increases upon increasing the magnetic field and reaches a value of 11.87 $N\beta$ at 7 T consistent with an S = 11/2 ground spin state. The magnetic study of **18**–**20** is consistent with ferromagnetic coupling between the metal ions. Ac susceptibility measurements of **18**–**20** between 1.8–10.0 K and frequencies 3–969 Hz under zero dc field showed temperature- and frequency-dependent out-of-phase peaks for **19** and **20** suggesting SMM behavior.

The relaxation time derived from the χ'' peaks follows the Arrhenius law $\tau = \tau_0 \exp(\Delta/k_B T)$ with effective energy barriers of 14.17 K ($\tau_0 = 1.09 \times 10^{-6}$ s) for **19** and 11.13 K ($\tau_0 = 6.72 \times 10^{-6}$ s) for **20** under zero dc field. Complexes **19** and **20** constitute rare examples of SMMs containing six-coordinate Dy^{III} ions.

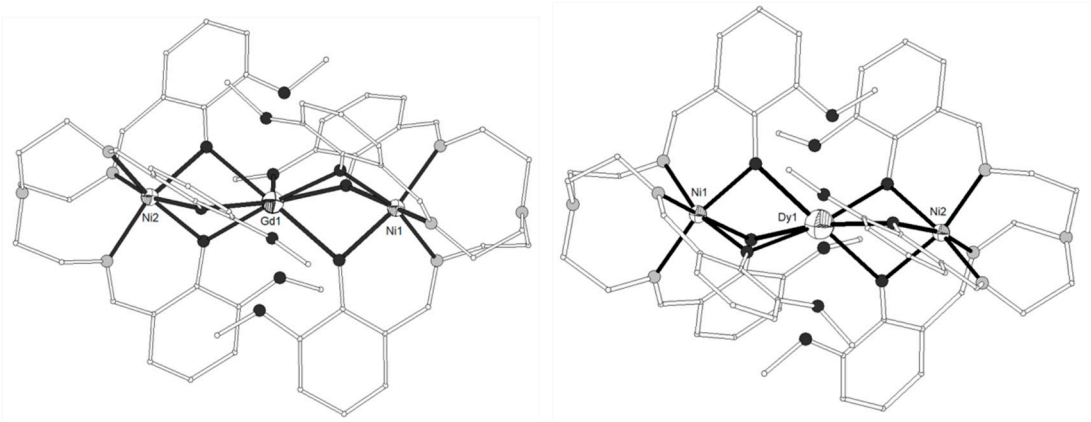

Figure 3. The molecular structures of the cations $[(NiL^4)_2Gd]^+$ (**17**, **left**) and $[(NiL^4)_2Dy]^+$ (**20**, **right**). Color code as in Figure 2 [22].

The tripodal hexadentate amine phenol ligand H_3L^5 = 2,2′-(((2-(((2-hydroxybenzyl)amino)methyl)-2-methylpropane-1,3-diyl)bis(azanediyl))bis(methylen e))diphenol (Scheme 1), which is the reduced form of ligand H_3L^2, gave a series of isostructural complexes $[(NiL^5)_2Ln(solv)_x)](ClO_4)$ (Ln^{III} = La, Pr, Nd, Gd, Dy, Ho, Er, Yb; **21**–**28**; x = 2, $H_2O/(MeOH)_{0.5}/(EtOH)_{0.5}$ in Ni_2La, **21**; x = 2, H_2O/MeOH in Ni_2Dy, **25**; x = 1, H_2O in Ni_2Yb, **28**) [23]. The complexes consist of two $[NiL^5]^-$ metalloligands bound around the Ln^{III} ions with bent Ni-Ln-Ni moiety. The La^{III} ion in **21** is eight-coordinate to two $(L^5)^{3-}$ ligands which are tridentate with respect to the La^{III} ion and hexadentate with respect to one Ni^{II} ion (Figure S2). Two solvate molecules complete the coordination of the La^{III} ion which is described as a D_{4d} square antiprism distorted toward a C_{2v} bicapped octahedron. The Dy^{III} ion is seven-coordinate to two $[NiL^5]^-$ metalloligands, one bidentate and one tridentate and to two solvate molecules in a capped trigonal prismatic geometry. The Yb^{III} ion is six-coordinate to two $[NiL^5]^-$ metalloligands with a distorted octahedral geometry. The magnetic studies indicated that antiferromagnetic exchange coupling between the Ni^{II} and Ln^{III} ions increases with decreasing size of Ln^{III}.

The tripodal hexadentate amine phenol ligand H_3L^6 = 2,2′,2′′-(((nitrilotris(ethane-2,1-diyl))tris (azanediyl))tris(methylene))triphenol (Scheme 1) gave two series of isostructural complexes, $[(NiL^6)_2Ln(MeOH)](NO_3)$ (all Ln^{III} except Ce and Pm, **29**–**41**) and $[(NiL^6)_2Ln(MeOH)](ClO_4)$ (Ln^{III} = La, Pr, Nd, Sm, Gd, Dy, Ho, Er, **42**–**49**), which contain a bent Ni-Ln-Ni moiety with angles in the range ~139–144° [24,25]. In all structurally characterized complexes, the Ln^{III} ion is seven-coordinate being bicapped by two tridentate $[NiL^6]^-$ metalloligands and a methanol molecule in flattened pentagonal bipyramidal geometry. Each Ni^{II} ion is encapsulated by a full deprotonated ligand via four amine and two phenolato functions in approximately octahedral geometry (Figure S3). It is recognized that the coordination number of Ln^{III} ions tends to decrease with increased atomic number, that is, as the ionic radius decreases. However, in the present case, the coordination number and geometry of the Ln^{III} ions do not change along the entire Ln series plus La^{III}. Magnetic studies indicated that ferromagnetic exchange occurs in the case of Ni_2Ln with Ln^{III} = Gd, Tb, Dy, Ho, Er.

The congener ligand H_3L^7 = 6,6′,6′′-(((nitrilotris(ethane-2,1-diyl))tris(azane diyl))tris(methyl ene))tris(2-methoxyphenol) (Scheme 1) gave two isomorphous complexes $[(NiL^7)_2Ln)](ClO_4)$ (Ln^{III} = Gd, Dy, **50**–**51**) which contain a bent Ni-Ln-Ni moiety with angle ~113° [26]. The three metal ions are arranged in an isosceles triangle manner (Figure 4). The two terminal Ni^{II} ions are coordinated to four amine and two phenolate groups, whereas the central Ln^{III} ion is eight-coordinated to six

bridging phenolato oxygen atoms and two methoxy oxygen atoms from the ligands presenting distorted dodecahedral geometry. The magnetic studies showed that both complexes exhibit ferromagnetic coupling between the metal ions. The magnetic susceptibility data of **50** were analyzed on the basis of the spin Hamiltonian $\hat{H} = -2J\left(\hat{S}_{Ni1}\hat{S}_{Gd} + \hat{S}_{Gd}\hat{S}_{Ni2}\right) - 2J'\hat{S}_{Ni1}\hat{S}_{Ni2}$ (J' is assumed to be zero due to large distance between the Ni^{II} ions) and gave J/k = 1.02 cm^{-1} and g = 2.01. At 2 K, the magnetization is 11.04 $N\beta$ at 5 T which agrees with the saturation value of 11.94 $N\beta$ expected for an S = 11/2 system, confirming the ferromagnetic interaction between the Ni^{II} and Gd^{III} ions. The magnetization at 5 T for **51** is 12.65 $N\beta$ and is larger than the theoretical value of 12 $N\beta$ due to the presence of the anisotropic Dy^{III} ion. The Ni_2Dy complex **51** exhibited very weak field-induced slow relaxation of magnetization.

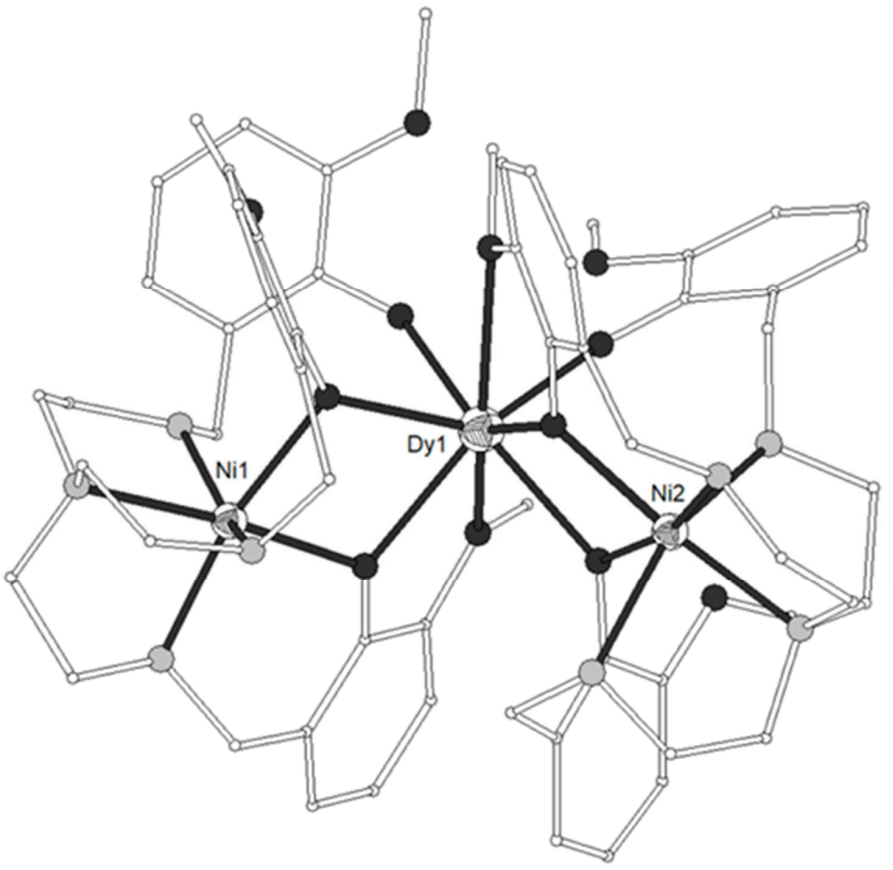

Figure 4. The molecular structure of the cation $[(NiL^7)_2Dy)]^+$ in complex **51**. Color code as in Figure 2 [26].

The ligand H_3L^8 = 2,2′,2′′-((1,4,7-triazonane-1,4,7-triyl)tris(methylene))triphenol (Scheme 1) gave the trinuclear complexes $[(NiL^8)_2Ln(MeCN)_2](ClO_4)$ (Ln^{III} = La, Nd, Gd, Dy, Yb, **52**–**55**) and $[(NiL^8)_2Yb](ClO_4)$ (**56**) [27]. The Gd^{III} ion in **54** is eight-coordinate in square antiprism distorted to C_{2v} bicapped trigonal prism geometry, bicapped by two deprotonated tridentate $(NiL^8)^-$ metalloligands (Figure 5). Each Ni^{II} is distorted octahedral in N_3O_3 coordination. The Ni-Gd-Ni angle is ~142°. The Yb^{III} ion in **56** is six-coordinated by six bridging phenolate oxygens (Figure 8). The decrease of the coordination number with increasing atomic number is common in Ln^{III} complexes. The complex is linear with Ni-Yb-Ni angle ~176°. Magnetic studies indicated ferromagnetic interactions for Ln^{III} = Gd, Dy, Yb and antiferromagnetic coupling for Ln^{III} = Nd.

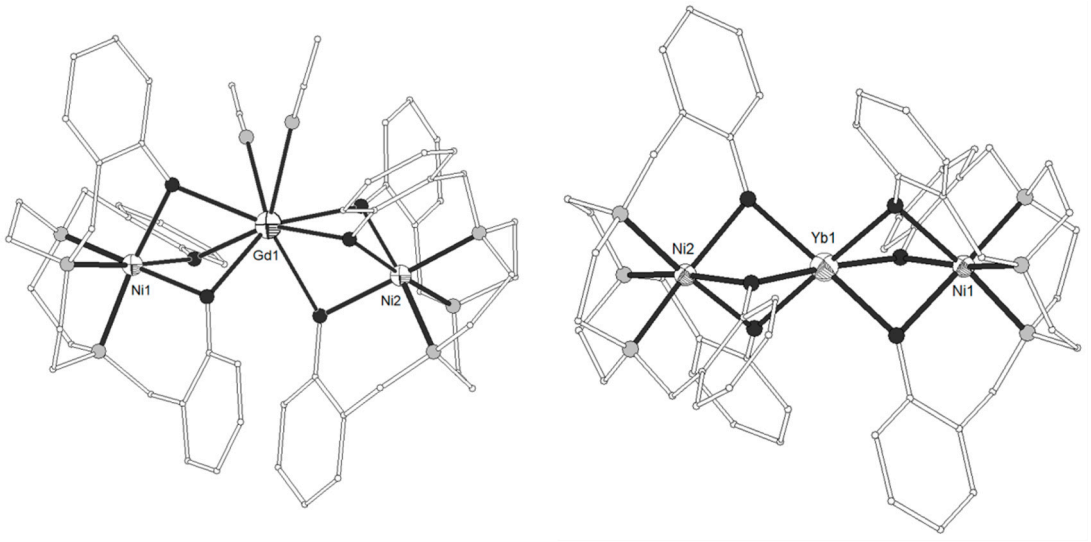

Figure 5. The molecular structures of the cations $[(NiL^8)_2Gd(MeCN)_2]^+$ **54**, (**left**) and $[(NiL^8)_2Yb]^+$ **56**, (**right**). Color code as in Figure 2 [27].

The ligand H_3L^9 = 6,6′,6′′-((1,4,7-triazonane-1,4,7-triyl)tris(methylene))tris(2-methoxy-3-methylphenol) (Scheme 1) gave a series of 13 linear trinuclear complexes $[(NiL^9)_2Ln(solv)_x](ClO_4)$ (Ln^{III} = Y, La, Ce-Lu except Pr, Pm, Yb; x = 1, H_2O in Ni_2Sm, Ni_2Eu, Ni_2Tb; x = 0 in all other complexes, **57**–**69**) [28]. For complexes with Ln^{III} = Sm, Eu, Tb, the central lanthanide is seven-coordinate showing monocapped trigonal prismatic geometry (Figure S4). For the rest of the complexes, the central lanthanide as well as the terminal Ni^{II} ions are six-coordinate with coordination geometry between trigonal antiprism and trigonal prism and distorted octahedral, respectively. The Ni-Ln-Ni angles are in the range 165–179°. For **57**, **58** and **69** the $\chi_M T$ at 300 K is 2.48 cm^3Kmol^{-1}, 2.33 cm^3Kmol^{-1} and 2.76 cm^3Kmol^{-1}, higher than the theoretically expected value of 2.0 cm^3Kmol^{-1} because the diamagnetic Ln^{III} ions may induce small geometric variations and different ligand fields at the Ni^{II} ions, thus affecting the magnetic properties of the three complexes. The reduced magnetization for **57** and **69** shows a splitting of the isofield lines, which indicates a zero-field splitting. The best fit leads to $J_{Ni\text{-}Ni}$ = −0.294 cm^{-1}, g_{Ni} = 2.09, D_{Ni} = 1.933 cm^{-1} and E/D = 0.154 for **57** and $J_{Ni\text{-}Ni}$ = −0.129 cm^{-1}, g_{Ni} = 2.18, D_{Ni} = 2.838 cm^{-1} and E/D = 0.468 for **69**. The fit of the magnetic data of the Ni_2Gd complex **63** gave $J_{Ni\text{-}Ni}$ = −0.377 cm^{-1}, $J_{Gd\text{-}Ni}$ = −0.009 cm^{-1}, g_{Ni} = 2.102, g_{Gd} = 1.974 and χ^{TIP} = 0.003 cm^3Kmol^{-1}. Paramagnetic nuclear magnetic resonance (NMR) spectroscopy showed that in solution all complexes are isostructural showing the expected D_3 symmetry for all metal ions being six-coordinate. These complexes have small magnetic anisotropies and the NMR data agree with the solid state SQUID measurements.

The ligand H_3L^{10} = 6,6′,6′′-((1,4,7-triazonane-1,4,7-triyl)tris(methylene))tris(2,3-dimethylphenol) (Scheme 1) was used to prepare the linear complex $[(NiL^{10})_2Tb](ClO_4)$ (**70**) [29]. Each Ni^{II} ion is coordinated by three nitrogen and three phenolate oxygen atoms in octahedral geometry and the Tb^{III} ion is bound to six phenolate oxygen atoms in octahedral geometry also (Figure S5). The magnetic studies revealed ferromagnetic interactions between the adjacent Ni^{II} and Tb^{III} ions.

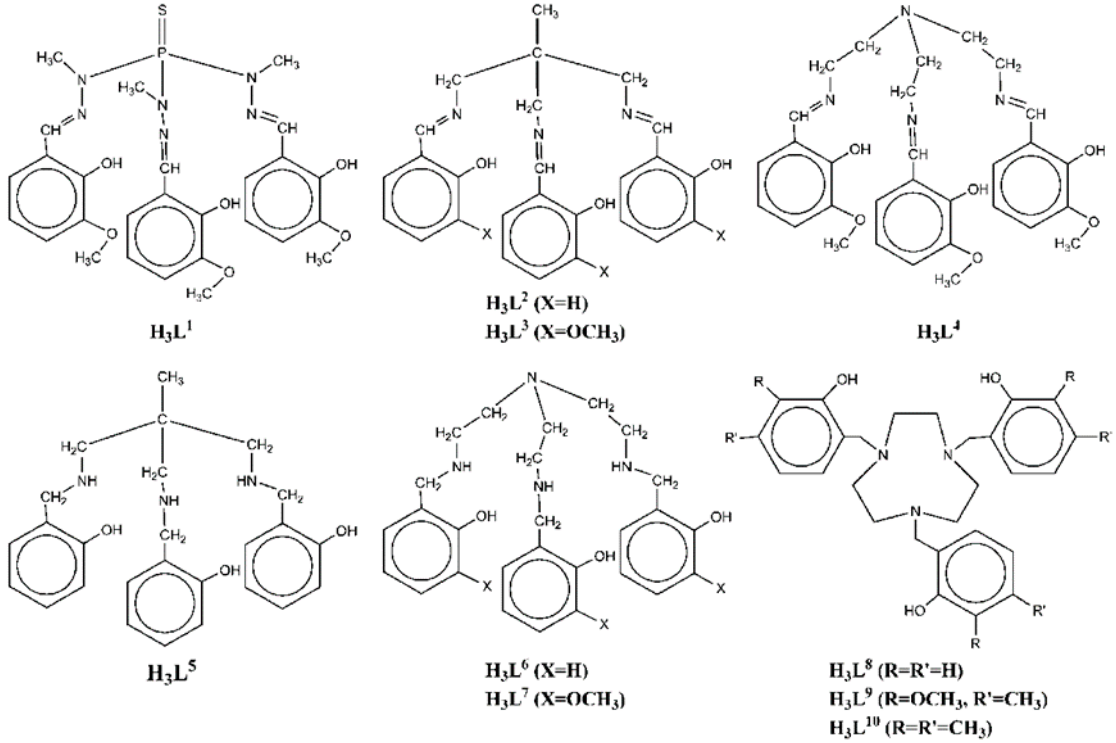

Scheme 1. The tripodal polydentate Schiff base and reduced Schiff base ligands used in the Ni_2Ln complexes **1**–**70**.

2.1.2. Other Schiff Base Ligands

The Schiff base ligand HL^{11} = (*Z*)-2-methoxy-6-((phenylimino)methyl)phenol (Scheme 2) derived from the condensation of *o*-vanillin with aniline, gave the linear trinuclear complexes $[(NiL^{11}{}_3)_2Ln](NO_3)$ (Ln^{III} = La, Pr, Gd, Tb, **71**–**74**) [30,31] which contain two terminal Ni^{II} ions in octahedral N_3O_3 coordination and a central Ln^{III} ion bound to six phenolato and six methoxy oxygen atoms from six $(L^{11})^-$ ligands. The central Ln^{III} ion sits on inversion center and displays distorted icosahedron geometry (Figure 6). The Ni_2Gd complex **73** displays ferromagnetic coupling giving a ground spin state value of S = 11/2. Simultaneous fitting to $\chi_M T(T)$ and isothermal $M(H)$ plots by using the spin Hamiltonian $H = -2J_1(S_{Ni1}S_{Gd1} + S_{Gd1}S_{Ni1A})$ and considering a single unique Ni-Gd interaction J_1, gave J_1 = +0.54 cm^{-1} with fixed g = 2.01. Q-band EPR spectra of polycrystalline **73** at 5 K can be reproduced by a model with S = 11/2 and ZFS parameters D = −0.135 cm^{-1}, E/D = 0.004 with g = 2.05. The magnetocaloric efficiency of the Ni_2Gd cluster **73** was studied for the first time for a linear Ni_2Gd cluster, via heat capacity and isothermal magnetization measurements which revealed a value of 13.74 $Jkg^{-1}K^{-1}$ for the magnetic entropy change at 4 K and ΔH = 7 T. Weak ferromagnetic exchange between the Ni^{II} ions is found in the Ni_2La complex **71**. The experimental data were fitted by considering the spin Hamiltonian $H = -2JS_{Ni1}S_{Ni2} + 2D_{Ni}S^2_{Niz}$ considering the zero-field splitting parameter D and gave J = +0.46 cm^{-1}, g = 2.245, D = +4.91 cm^{-1}. Dc magnetic susceptibility measurements revealed that the Ni^{II} ions are coupled ferromagnetically with the Tb^{III} ion in **74** and antiferromagnetically with the Pr^{III} ion in **72**. Ac susceptibility measurements performed on the Ni_2Tb complex **74** under zero dc field and under H = 0.5 T revealed the onset of frequency dependent χ''_M signals indicating the possibility of SMM behavior. The absence of clear maxima in the $\chi''_M(T)$ plots down to 2 K indicates fast magnetic relaxation or fast QTM or perhaps both.

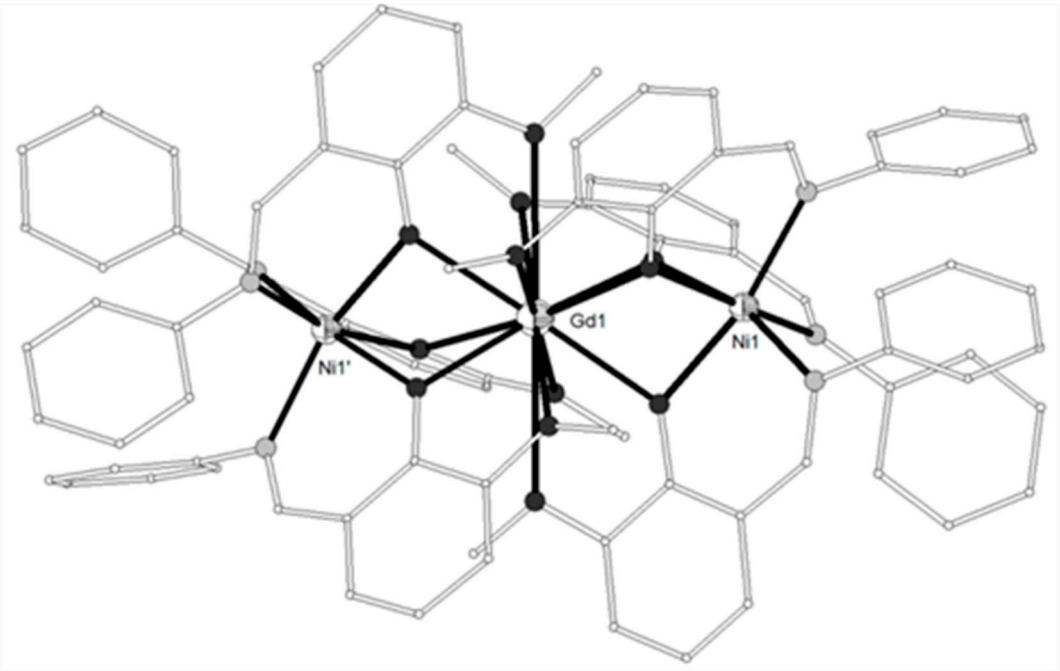

Figure 6. The molecular structure of the cation $[(NiL^{11}{}_3)_2Gd]^+$ in complex **73**. Primed atoms are generated by symmetry (′) 1−*x*, *y*, 0.5−*z*. Color code as in Figure 2 [30].

The Schiff base ligand H_2L^{12} = (*Z*)-2-(((2-(hydroxymethyl)phenyl)imino)methyl)-6-methoxyphenol (Scheme 2) gave, among others, the linear trinuclear complex $[\{Ni(HL^{12})_2\}_2La(NO_3)](NO_3)_2$ (**75**) which contains two Ni^{II} ions in distorted octahedral N_2O_4 environment and a central La^{III} ion bound to four phenolato and four methoxy oxygen atoms from four $(HL^{12})^-$ ligands and two oxygen atoms from a chelate nitrate (Figure S6) [32]. The coordination geometry around the La^{III} ion is best described as sphenocorona JSPC-10 (CShM = 3.37915). Weak antiferromagnetic exchange between the Ni^{II} ions is found in the complex via the closed shell La^{III} ion. The fit of the $\chi_M T$ data from 150 K to 2 K using a HDVV Hamiltonian yielded parameters $J = -0.978$ cm^{-1}, $g = 2.177$, $D = 3.133$ cm^{-1}.

The pentadentate Schiff base ligand H_4L^{13} = (*Z*)-2-((2-hydroxy-3-(hydroxymethyl)-5-methylbenzylidene)amino)-2-methylpropane-1,3-diol (Scheme 2) was used to prepare a family of isostructural complexes $[\{Ni(H_3L^{13})_2\}_2Ln](NO_3)_3$ (Ln^{III} = Gd, Tb, Dy, Ho, **76**–**79**) with linear metal arrangement (Figure 7) [33]. Each of the terminal Ni^{II} ions is distorted octahedral in N_2O_4 environment; the four oxygen atoms are derived from two phenolates and two pendant -CH_2OH arms of the two different $(H_3L^{13})^-$ ligands. The two imino nitrogen atoms around Ni are *trans* with respect to each other. The central Ln^{III} ion is coordinated to eight oxygen atoms (four benzyl alcohol groups and four phenolato O-atoms) in square antiprismatic geometry. Each Ni_2Ln complex interacts with four neighboring molecules through the -CH_2OH groups of the ligands and the NO_3^- counteranions, leading to 2D H-bonded network along the *ab* plane. The static magnetic properties of all four complexes showed a predominant ferromagnetic interaction between the metal ions and only the Ni_2Dy complex exhibited frequency dependent tails in the χ''_M *vs T* plots under zero dc field. The magnetic properties of complex **76** were analyzed by using the spin Hamiltonian $H = -J_{ex}(S_{Ni1}S_{Gd} + S_{Ni2}S_{Gd}) - D\left(S_z^2Ni1 + S_z^2Ni2\right)$ assuming two equivalent $Ni(O)_2Gd$ bridging halves. The best-fit parameters are $J_{ex} = +0.67$ cm^{-1}, $g = 2.117$, $D = 4.92$ cm^{-1} ($R = 7 \times 10^{-7}$). The magnetocaloric properties of the Ni_2Gd were estimated from the experimental isothermal field-dependent magnetization data yielding $-\Delta S_m = 11.85$ Jkg^{-1}K^{-1} at 4 K and $\Delta H = 5$ T.

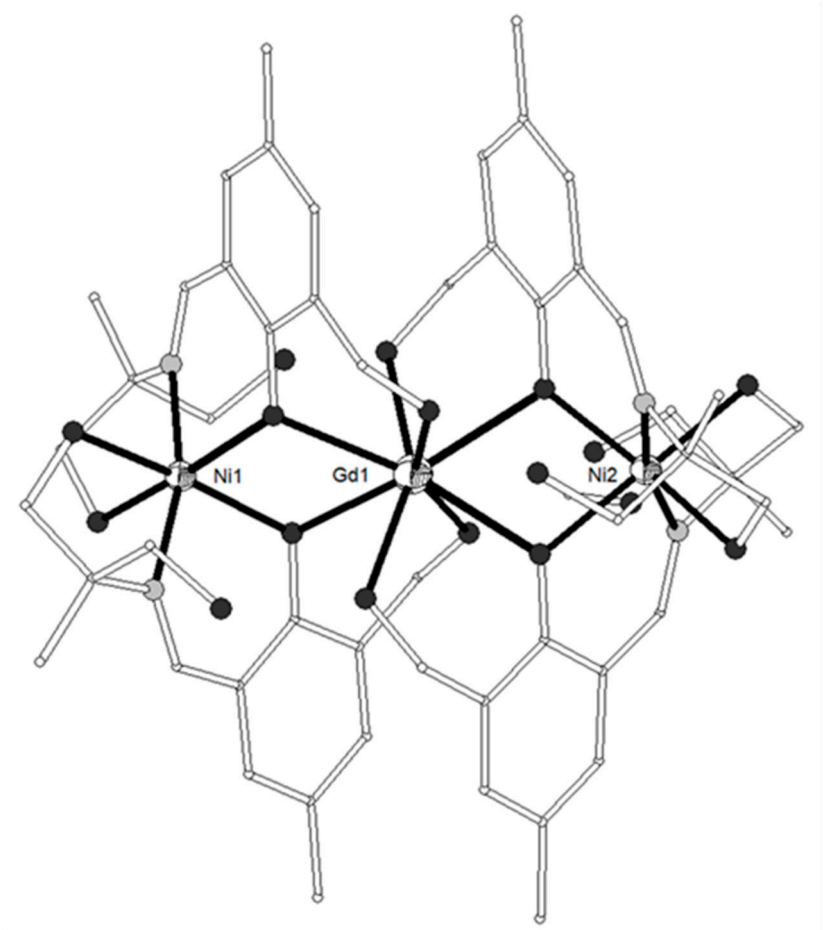

Figure 7. The molecular structure of the cation $[\{Ni(H_3L^{13})_2\}_2Ln]^{3+}$ in complex **76**. Color code as in Figure 2 [33].

The Schiff base ligand H_4L^{14} = (*Z*)-2-((2-hydroxybenzylidene)amino)-2-(hydroxymethyl)propane-1,3-diol (Scheme 2) afforded four isostructural complexes with formula $[\{Ni(H_3L^{14})_2\}_2Ln(O_2CMe)_2](NO_3)_3$ (Ln^{III} = Sm, Eu, Gd, Tb, **80**–**83**) with strictly linear metal arrangement (Figure 8) [34]. The two Ni^{II} ions display N_2O_4 distorted octahedral coordination and the central Ln^{III} ion is coordinated to four phenolato oxygen atoms from four $(H_3L^{14})^-$ ligands and four carboxylato oxygen atoms from two chelate acetates describing square antiprismatic geometry. The magnetic susceptibility data of **80** revealed weak antiferromagnetic coupling between the two Ni^{II} ions with best fit parameters $J = -0.37$ cm^{-1}, $g = 1.97$ and TIP = 0.001 cm^{3}mol^{-1}. The $\chi_M T$ product of **81** at 300 K is higher than expected and can be explained by assuming that the first excited states for the Eu^{III} ion are populated at r.t. because they are very close to the ground state. The magnetic susceptibility data of **82** revealed dominant ferromagnetic interactions between the Ni^{II} and Gd^{III} ions and were fitted by using the spin Hamiltonian $H = -2J_{NiGd}(S_{Ni1}S_{Gd} + S_{Ni2}S_{Gd}) + D\left(S_{Ni1}^2 + S_{Ni2}^2\right)$ yielding $J_{NiGd} = +0.42$ cm^{-1}, $D = +2.95$ cm^{-1} ($g_{Ni} = g_{Gd} = 1.98$), resulting in $S = 11/2$ spin ground state. The magnetocaloric effect of **82** was determined by isothermal magnetization measurements in the temperature range 2–12.5 K under applied magnetic fields up to 5 T with $-\Delta S_m = 14.2$ Jkg^{-1}K^{-1} at 2 K. The magnetic susceptibility data for **83** are consistent with dominant antiferromagnetic interactions between the metal ions and/or thermal depopulation of the Tb^{III} excited states.

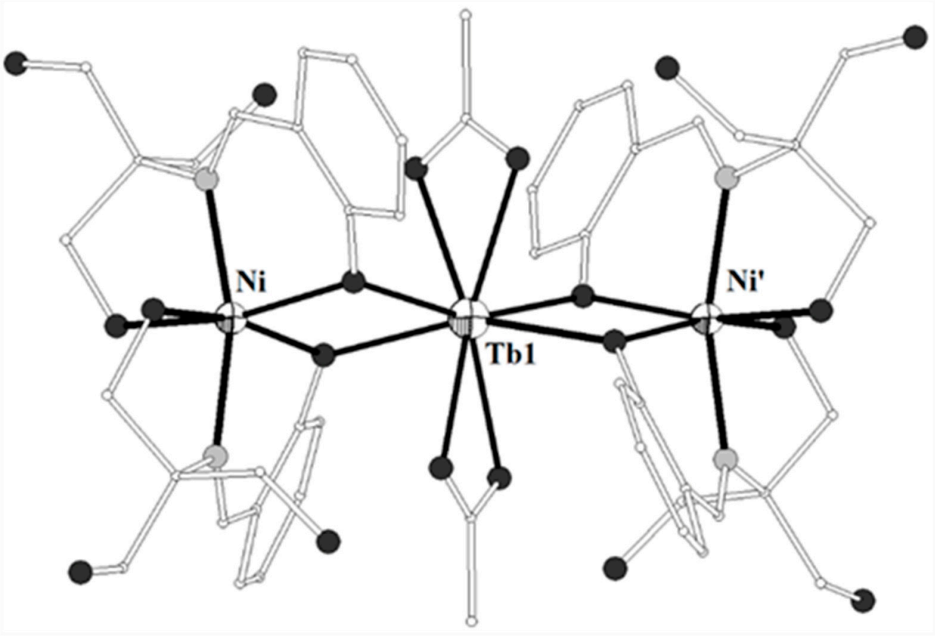

Figure 8. The molecular structure of the cation $[\{Ni(H_3L^{14})_2\}_2Ln(O_2CMe)_2]^+$ in complex **83**. Primed atoms are generated by symmetry: (′) 1.5−*x*, 0.5−*y*, *z*. Color code as in Figure 2 [34].

The hexadentate Schiff base ligand H_2L^{15} = 6,6′-((1*E*,1′*E*)-(ethane-1,2-diylbis(azanylylidene))bis (methanylylidene))bis(2-ethoxyphenol) (Scheme 2) gave two isostructural trinuclear complexes $[(NiL^{15})_2Ln(NO_3)_2](NO_3)$ (Ln^{III} = La, Ce, **84**–**85**) with bent Ni-Ln-Ni arrangement (Figure S7) [35]. The central Ln^{III} ion is bound to four phenolato and four ethoxy oxygen atoms as well as to two chelate NO_3^- anions in distorted icosahedron geometry. Each of the terminal Ni^{II} ions is coordinated to the two imino nitrogen and two phenolato oxygen atoms of the ligand in square planar geometry. The Ln^{III} ion is bridged to each of the Ni^{II} ions via two phenolato and two ethoxy oxygen atoms. Both complexes showed antimicrobial activity on cultures of *E. coli*, *S. aureus* and CA. The congener ligand H_2L^{16} (Scheme 2) gave a similar Ni_2Ce complex with Ni-Ce-Ni angle of ~62° [36].

The ligand H_2L^{17} = 6,6′-((1*E*,1′*E*)-(propane-1,3-diylbis(azanylylidene))bis(methanylylidene))bis (4-bromo-2-methoxyphenol) (Scheme 2) gave four isostructural trinuclear complexes $[(NiL^{17})_2Ln(O_2CMe)_2(MeOH)_2](NO_3)$ (Ln^{III} = La, Nd, Ce, Pr, **87**–**90**) [37,38] which contain a central Ln^{III} ion in an inversion center bound to four phenolato and four methoxy oxygen atoms as well as to two acetato oxygen atoms from two carboxylato ligands in pentagonal antiprismatic geometry (Figure 9). Each Ni^{II} ion occupies the N_2O_2 compartment of the ligand and has distorted octahedral geometry with MeOH and bridging acetato oxygen atoms in the apical positions. The Ln^{III} ion is bridged to each of the Ni^{II} ions via the two phenolato oxygen atoms and the acetato group. Weak antiferromagnetic coupling between the Ni^{II} ions through the diamagnetic La^{III} ion was found in the Ni_2La complex **87**. The magnetic susceptibility data were interpreted based on the isotropic Heisenberg model ($H = -2J\vec{S}_{Ni1}\vec{S}_{Ni2}$) and the best least-squares fit yielded $J = -0.75$ cm^{-1}, $g = 2.18$. The susceptibility data of the Ni_2Nd, Ni_2Ce and Ni_2Pr complexes **88**, **89**, **90** respectively obey the Curie-Weiss law with the Curie constant of $C = 3.71$ cm^3 K mol^{-1} and the Weiss constant of $\theta = -7.4$ K for **88**, $C = 3.23$ cm^3 K mol^{-1} and $\theta = -9.9$ K for **89** and $C = 4.05$ cm^3 K mol^{-1} and $\theta = -25.5$ K for **90**. The negative values of Weiss constant confirm the antiferromagnetic exchange coupling between the metal ions. For complexes **89** and **90**, the crystal field parameters for the Ce^{III}/Pr^{III} ions and the exchange coupling constant were estimated by using the generalized van Vleck formalism. The best fit yielded $J_{NiCe} = -1.1(4)$ cm^{-1}, $g_{Ni} = 2.23(3)$, $D = 6.3(4)$ cm^{-1}, $A^0_2\langle r^2\rangle = -265(10)$ cm^{-1}, $A^0_4\langle r^4\rangle = 291(6)$ cm^{-1} for **89** and $J_{NiPr} = -1.3(8)$ cm^{-1}, $g_{Ni} = 2.15(2)$, $D = 7.1(4)$ cm^{-1}, $A^0_2\langle r^2\rangle = -310(9)$ cm^{-1}, $A^0_4\langle r^4\rangle = 2335(11)$ cm^{-1}, $A^0_6\langle r^6\rangle = 80(8)$ cm^{-1} for **90.**

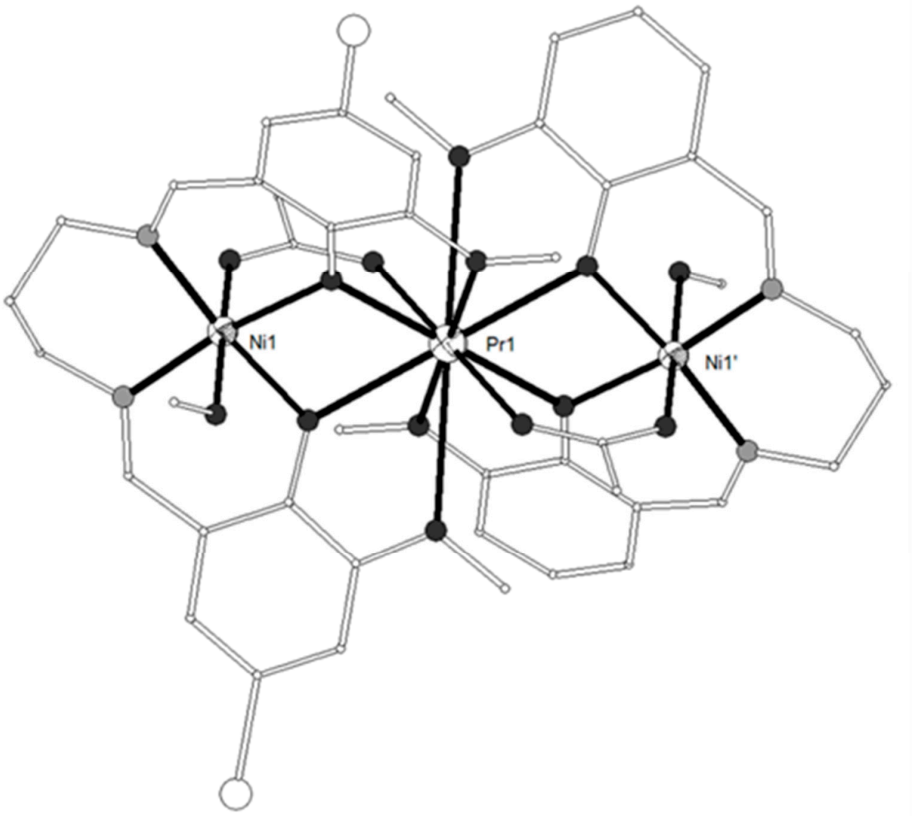

Figure 9. The molecular structure of the cation $[(NiL^{17})_2Pr(O_2CMe)_2(MeOH)_2]^+$ in complex **90**. Primed atoms are generated by symmetry: (') 1−*x*, 1−*y*, 1−*z*. Color code: Gd large octant, Ni small octant, N light grey, O dark grey, C open small, Br open large [38].

The tetradentate Schiff base ligand H_2L^{18} = 2,2′-((1*E*,1′*E*)-(propane-1,3-diylbis (azanylylidene)) bis(ethan-1-yl-1-ylidene))diphenol (Scheme 2) gave a trinuclear complex $[(NiL^{18})_2Ce(NO_3)_3]$ (**91**) with a central Ce^{III} ion bound to two terminal [Ni(L^{18})] metalloligands in a *transoid* orientation to the central lanthanide ion (Figure S8) [39]. The Ce^{III} ion is ten-coordinate to four phenolato oxygen atoms and to three chelate nitrates, the coordination polyhedron can be described as distorted tetradecahedron. Each Ni^{II} ion is in N_2O_2 square planar geometry. The Ni-Ce-Ni moiety is bent with angle ~122.5°.

The ligand H_2L^{19} = 6,6′-((1*E*,1′*E*)-((2,2-dimethylpropane-1,3-diyl)bis(azanyl ylidene))bis(methanyl ylidene))bis(2-methoxyphenol) (Scheme 2) gave the trinuclear complexes $[\{NiL^{19}(H_2O)\}_2Ln(H_2O)](trif)_3$ (Ln^{III} = Gd, Eu, **92**–**93**; trif = triflate anion) which contain a nine-coordinate central Ln^{III} ion bound to four phenolato and four methoxy oxygen atoms from two $(L^{19})^{2-}$ ligands and a water molecule (Figure 10) [21,40]. Each of the terminal Ni^{II} ions is five-coordinate, linked to the N_2O_2 site of the ligand in the equatorial plane and to a water molecule in the apical position. The magnetic susceptibility data of **92** were fitted considering two different *J* parameters for the Ni-Gd magnetic exchange and an equivalent *D* term for both nickel ions, according to the spin Hamiltonian $H = -J_{NiGd}(S_{Ni1}S_{Gd}) - j_{NiGd}(S_{Ni2}S_{Gd}) + D\left(S_z^2Ni1 + S_z^2Ni2\right)$. The best fit yielded J_{NiGd} = 4.8(3) cm^{-1}, j_{NiGd} = 0.05(2) cm^{-1}, *g* = 2.03(1) and *D* = 0.03(1) cm^{-1} ($R = 1 \times 10^{-5}$). A very similar *J* value (0.5 cm^{-1}) yielded when the data were fitted without *j* and *D* parameters. The observed magnetization of 9.3 *Nβ* at 5 T was explained considering a ferromagnetic Ni-Gd dinuclear unit plus a mononuclear pentacoordinate Ni ion having a large magnetic anisotropy due to zero field splitting. The magnetization curve was fitted with *J* = 5 cm^{-1}, *j* = 0, *D* = 12.4 cm^{-1}, g_{Ni} = 2.16 and g_{Gd} = 2.00. The magnetic susceptibility data of **93** is governed by at least two magnetic phenomena that is, the depopulation of the Stark levels of the Eu^{III} ion and the zero-field splitting of the Ni^{II} ions at very low temperatures.

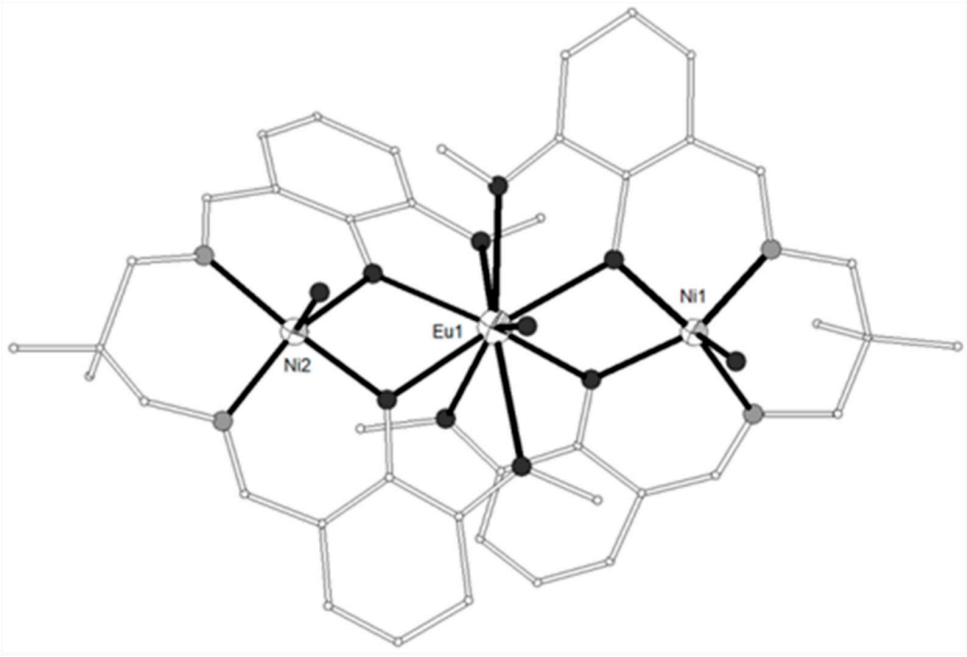

Figure 10. The molecular structure of the cation $[\{NiL^{19}(H_2O)\}_2Eu(H_2O)]^{3+}$ in complex **93**. Color code as in Figure 2 [40].

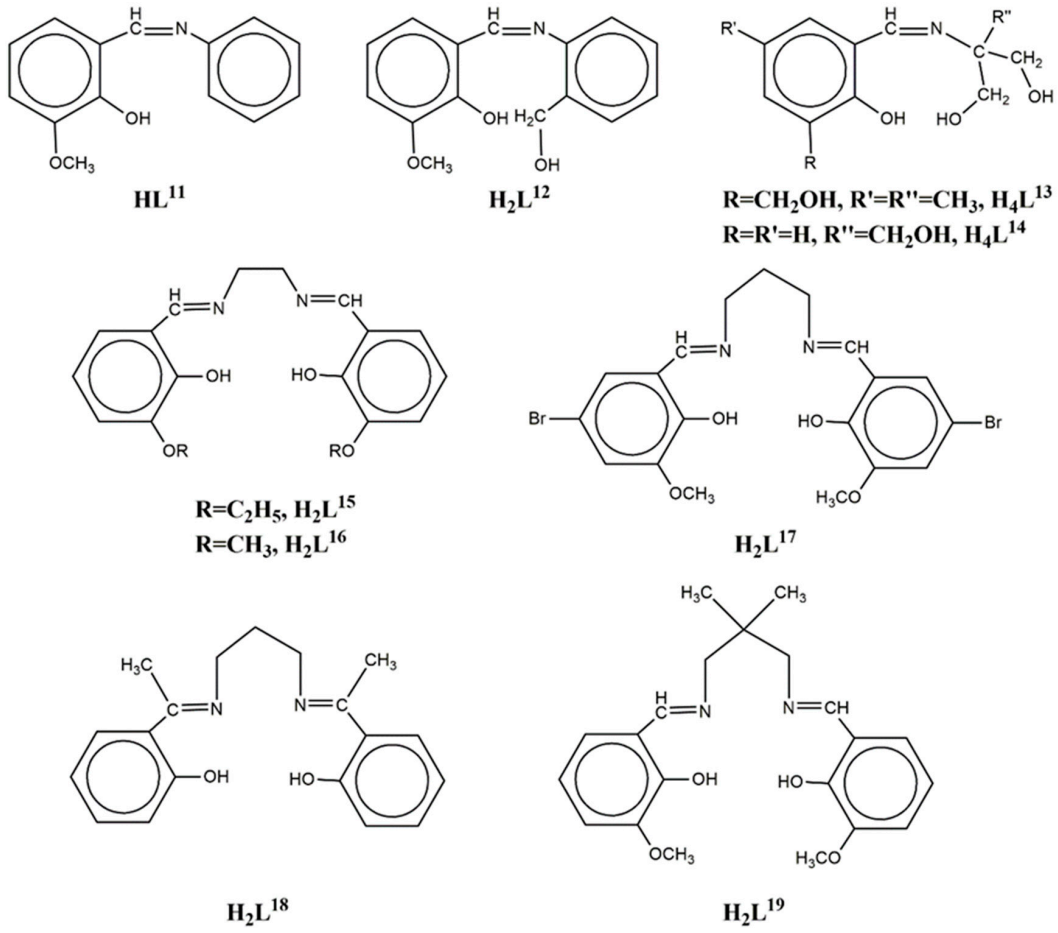

Scheme 2. The Schiff base ligands used in Ni_2Ln complexes **71**–**93**.

2.1.3. Miscellaneous Ligands

The dipodal Schiff base ligand H_4L^{20} = 3,3′-((1*E*,1′*E*)-((((2-aminoethyl)azanediyl)bis(ethane-2,1-diyl))bis(azanylylidene))bis(methanylylidene)) bis(2-hydroxybenzoic acid) (Scheme 3) gave a family of isomorphous V-shaped trinuclear complexes, $[\{Ni(H_2L^{20})(tren)_2\}_2Ln](NO_3)_3$ [Ln^{III} = Gd, Dy, Er, Lu, **94**–**97**; tren = tris(2-aminoethyl)-amine) [41]. The ligand was prepared in situ and this fact justifies the complexation of tren around the Ni^{II} ions (Figure 11). The Ln^{III} ions are eight-coordinate by four phenolato and four carboxylato oxygen atoms from two different ligands in distorted square antiprismatic geometry. Each of the terminal Ni^{II} ions is bound to four nitrogen atoms from the tren ligand, one amino group and one carboxylato oxygen atom from the Schiff base ligand in distorted octahedral geometry. Magnetic studies on all four complexes suggest the presence of weak antiferromagnetic interactions between neighboring ions. The magnetic susceptibility data of the Ni_2Gd complex **94** were interpreted considering the spin Hamiltonian $H = -2J(S_{Ni1}S_{Gd} + S_{Gd}S_{Ni2}) + 4\left[D_{Ni}\left(S_z^2 - \frac{1}{3}S(S+1)\right) + g_{Ni}\mu_B HS_z\right]$. The best set of parameters obtained using this model is J/k_B = −0.083 cm^{-1} and g = 2.03. In complex **97**, the two Ni^{II} ions are linked by the diamagnetic Lu^{III} ion and the magnetic susceptibility data were interpreted using the spin Hamiltonian $H = 2\left[D\left(S_z^2 - \frac{1}{3}S(S+1)\right) + g\mu_B HS_z\right]$ considering the axial single-ion zero-field splitting of the two Ni^{II} ions. The data were correctly fitted with D = 3.2(0) K and g = 2.19(2). The fit of the magnetic susceptibility data for **95** and **96** in the range 50–300 K to the Curie-Weiss law gave Curie constant C of 16.19 and 14.42 cm^3 K mol^{-1} and Weiss temperature θ of −4.2 and −7.9 K for **95** and **96** respectively. The negative θ value indicates the presence of antiferromagnetic interactions within the Ni^{II}-Ln^{III}-Ni^{II} moiety.

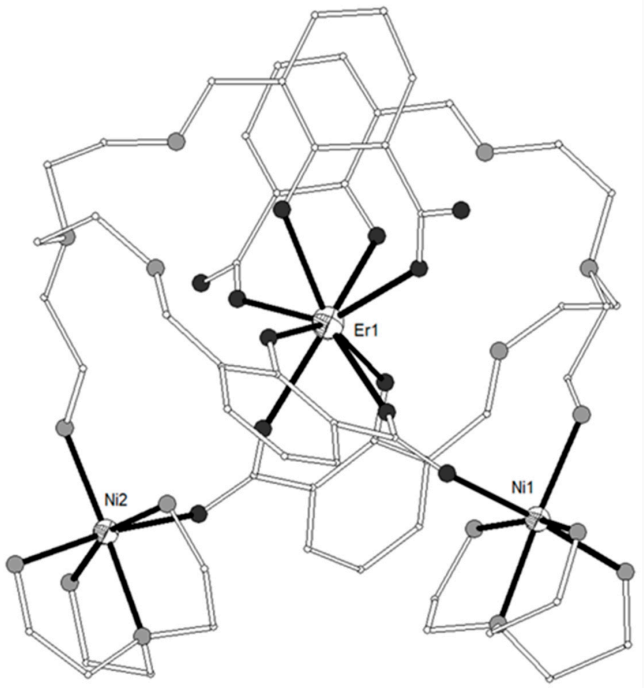

Figure 11. The molecular structure of the cation $[\{Ni(H_2L^{20})(tren)_2\}_2Er]^{3+}$ in complex **96**. Color code as in Figure 2 [41].

The ligand 8-hydroxyquinoline, HL^{21} (Scheme 3) gave the trinuclear complex $[\{Ni(L^{21})_3\}_2La(L^{21})]$, **98** (Figure S11) [42]. The two Ni^{II} ions are six-coordinate with distorted *fac*-octahedral coordination geometry derived from three chelating $(L^{21})^-$ ligands (O,N). The La^{III} ion is eight-coordinate with distorted square antiprismatic geometry bound to six bridging oxygen atoms of six $(L^{21})^-$ ligands and to a chelate $(L^{21})^-$ ligand through the nitrogen and oxygen atoms. The three metal ions form an angle of ~130°.

The ligand H_2L^{22} = 7,7′-(ethane-1,1-diyl)bis(quinolin-8-ol) (Scheme 3) was formed in situ under the solvo(hydro)thermal conditions used to prepare complexes [{Ni(L^{22})$_{1.5}$}$_2$Ln(OH)] (Ln^{III} = Eu, Tb, Gd, **99**–**101**) from 8-hydroxyquinoline as proligand (Figure S12) [43]. All complexes are isomorphous and crystallize in the hexagonal space group $P6_3/m$. The Ln^{III} ion has position occupation 0.16667 and presents tricapped trigon-prismatic geometry comprised six oxygen atoms from three ligands and three terminal OH^- groups with 0.16667 position occupation. The one crystallographically independent Ni^{II} ion has position occupation 0.33333 and is coordinated to three oxygen and three nitrogen atoms from three ligands creating a regular trigon-antiprismatic geometry. Supramolecular C-H···π interactions between neighboring molecules result in an overall 3D net. The dc susceptibility studies of the Ni_2Tb complex **100** displayed paramagnetic behavior in the temperature range 300–12.5 K and below that temperature a slow decrease in the $\chi_M T$ product mainly due to the thermal depopulation of crystal field effect.

The ligand HL^{23} (Scheme 3) was formed in situ via transition metal promoted nucleophilic addition of methanol to a nitrile group of dicyanonitrosomethanide (dcnm) and gave two families of trinuclear complexes, (Me_4N)[{(Ni(L^{23})$_3$}$_2$Ln(L^{23})$_2$] (Ln^{III} = La, Ce, Pr, Nd, Sm, **102**–**106**) and (Et_4N)$_2$[{(Ni(L^{23})$_3$}$_2$Ln(dcnm)$_2$](ClO_4) (Ln^{III} = La, Ce, **107**–**108**) [44]. The two Ni^{II} octahedral metal sites are each coordinated by three $(L^{23})^-$ ligands which chelate through the nitrogen atoms of the nitroso and imine groups to form a [Ni(L^{23})$_3$]$^-$ metalloligand. The central Ln^{III} ion is bound to two [Ni(L^{23})$_3$]$^-$ metalloligands and presents ten-coordination completed by two $(L^{23})^-$ ligands or two unreacted $dcnm^-$ ligands, all of them bound via the N,O atoms of the nitroso group (Figure 12). The coordination geometry around the Ln^{III} ions is best described as sphenocorona JSPC-10. The Ni_2Ln moiety is bent in both type of complexes with Ni-Ln-Ni angle of ~142 and ~133° for (Me_4N)[{(Ni(L^{23})$_3$}$_2$Ln(L^{23})$_2$] and (Et_4N)$_2$[{(Ni(L^{23})$_3$}$_2$Ln(dcnm)$_2$](ClO_4) complexes, respectively. Variable temperature magnetic susceptibilities on these complexes revealed practically zero Ni-Ni exchange coupling in the Ni_2La complexes **102** and **107**, possible weak antiferromagnetic coupling in Ni_2Pr **104** and possible weak ferromagnetic coupling in the Ni_2Ce complexes **103** and **108** but thermal depopulation and ligand-filed effects on the central Ln^{III} ion, particularly for Sm^{III}, make the unambiguous assignment of ferro- versus antiferromagnetic coupling rather difficult. In any case the magnetic behavior of **102**–**108** is similar to those of congener complexes.

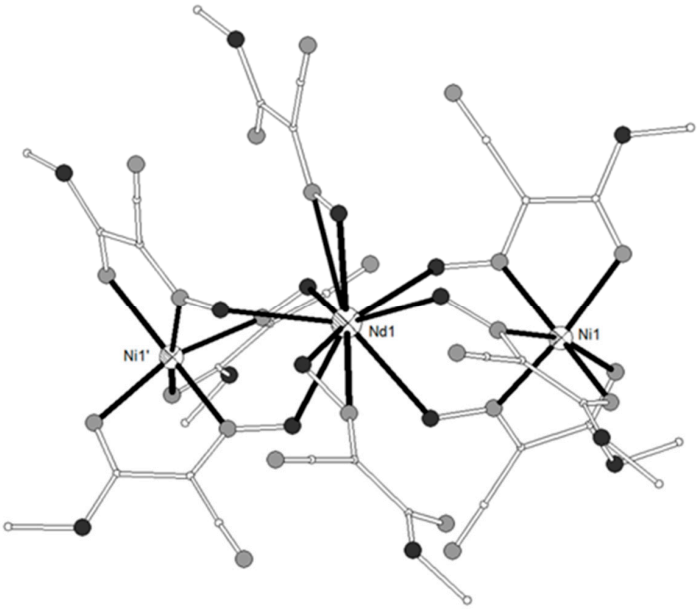

Figure 12. The molecular structure of the anion [{(Ni(L^{23})$_3$}$_2$Nd(L^{23})$_2$]$^-$ in complex **105**. Primed atoms are generated by symmetry: (′) 1/3 + y, −1/3 + x, 1/6 − z. Color code as in Figure 2 [44].

The ligand 2,6-di(acetoacetyl)pyridine, H_2L^{24} (Scheme 3) gave 18 trinuclear $Ni^{II}_2Ln^{III}$ complexes with Ln^{III} = La-Lu except for Pm, which crystallize in four different types: (A) $[(NiL^{24})_2Ln(NO_3)_2(MeOH)_4](NO_3)$ (Ln^{III} = La, Ce, Pr, Nd, Sm, Eu, Gd, **109–115**), (B) $[(NiL^{24})_2Ln(NO_3)_2(H_2O)_2(MeOH)_2](NO_3)$ (Ln^{III} = Sm, Eu, Gd, **116–118**), (C) $[(NiL^{24})_2Ln(NO_3)_3(MeOH)_4]$ (Ln^{III} = Gd, Tb, Dy, **119–121**) and (D) $[(NiL^{24})_2Ln(NO_3)_2(H_2O)(MeOH)_3](NO_3)$ (Ln^{III} = Ho, Er, Tm, Yb, Lu, **122–126**) [45]. All types of complexes are linear with Ni-Ln-Ni angles 180° (A), ~178° (B), ~173° (C) and ~179° (D). The two terminal Ni^{II} ions present O_6 distorted octahedral geometry bound to the 1,3-diketonate sites from two $(L^{24})^{2-}$ ligands together with MeOH and H_2O molecules. The central Ln^{III} ion is coordinated to the 2,6-diacylpyridine site from two $(L^{24})^{2-}$ ligands and to two or three nitrate ions in an overall ten-coordinate environment (Figure 13). The coordination geometry around the Ln^{III} ions is best described as hexadecahedron HD-10 in **109–115** and tetradecahedron TD-10 in **116–126**. The magnetic studies revealed that the Ni-Ln interaction is weakly antiferromagnetic for Ln = Ce, Pr, Nd and ferromagnetic for Ln = Gd, Tb, Dy, Ho, Er. The magnetic susceptibility data for **109** and **126** which contain the diamagnetic La^{III} and Lu^{III} ions, respectively, were interpreted based on the isotropic Heisenberg model $\hat{H} = -2JS_{Ni1}S_{Ni2}$. The best-fit parameters are $J = -0.63$ cm^{-1}, $g = 2.22$ for **109** and $J = -0.65$ cm^{-1}, $g = 2.17$ for **126**. For the Ni_2Gd complex, the spin Hamiltonian $\hat{H} = -2J(S_{Ni2}S_{Gd} + S_{Ni2}S_{Gd}) - 2J'S_{Ni1}S_{Ni2}$ (J is the exchange integral between the adjacent Ni^{II} and Gd^{III} ions and J' is the exchange integral between the terminal Ni^{II} ions) was used to fit the susceptibility data and considering $g_{Ni} = 2.20$ and $J' = -0.64$ cm^{-1} (the mean values for **109** and **126**) the best-fit parameters are $J = +0.79$ cm^{-1} $g_{Gd} = 2.02$. The magnetic data of the remaining complexes were evaluated by adopting an empirical method taking into account the behavior of the congener Zn_2Ln and Ni_2La complexes by using the equation $\Delta\chi_M T = \chi_M T(Ni_2Ln) - \chi_M T(Zn_2Ln) - \chi_M T(Ni_2La)$, $\Delta\chi_M T > 0$ for ferromagnetic and $\Delta\chi_M T < 0$ for antiferromagnetic interaction.

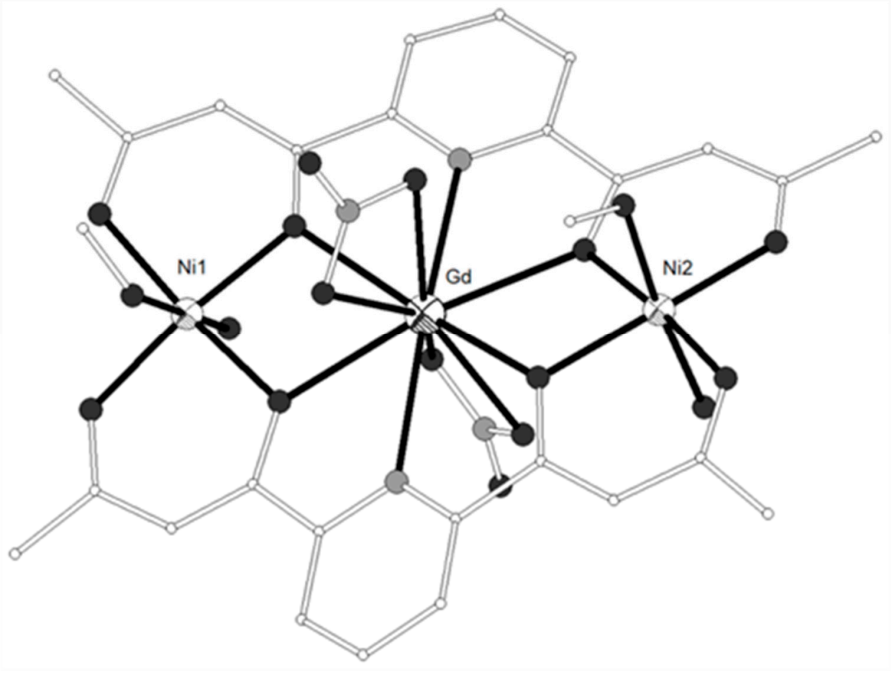

Figure 13. The molecular structure of the cation $[(NiL^{24})_2Gd(NO_3)_2(H_2O)_2(MeOH)_2]^+$ in complex **118**. Color code as in Figure 2 [43].

The congener ligand 2,6-bis(acetobenzoyl)pyridine H_2L^{25} (Scheme 3) gave the trinuclear complexes $[(NiL^{25})_2Ln(O_2CMe)_3(MeOH)_x]$ (Ln^{III} = Gd, Ce; x = 2 or 3, **127–128**) and $[(NiL^{25})_2Ln(O_2CPh)_3(solv)_x]$ (Ln^{III} = Gd, solv = MeOH, x = 2, **129**; Ce, solv = MeOH/H_2O x = 2, **130**) [46]. Each $(L^{25})^{2-}$ ligand is bound to the Ni^{II} sites through the 1,3-diketonate sites and to the central Ln^{III} ion through the

2,6-diacylpyridine site. Two carboxylato ligands act as bidentate bridging between the Ni^{II} and the Ln^{III} ions and the third act as chelate bidentate around the central lanthanide ion. The six-coordination around the Ni^{II} ions is completed by solvate molecules (Figure S13). The coordination number around the Ce^{III} ion is 10, whereas for the Gd^{III} is 9 or 10. The N_2O_7 nine-coordination around Gd^{III} in **127** is described as HH-9 (hula-hoop) and the N_2O_8 ten-coordination around the Ln^{III} ions in **128**–**130** is described as staggered dodecahedron SDD-10.

The ligand 2,6-dipicolinoylbis(N,N-diethylthiourea) H_2L^{26} (Scheme 3) gave the trinuclear complex $[(NiL^{26})_2Pr(O_2CMe)_3(MeOH)_2]$, **131** (Figure S14) [47]. The two Ni^{II} ions are bound to the S,O atoms from two $(L^{26})^{2-}$ ligands, one oxygen atom from the bridging acetato ligand and one methanol in distorted octahedral geometry. The Pr^{III} ion is ten-coordinate and is bound to the O,N,O group of the 2,6-diacylpyridine site of each $(L^{26})^{2-}$ ligand, two bridging and one chelate acetato groups. The polyhedron around the Pr^{III} ion is described as double-capped square antiprism.

The neutral trinuclear complexes $[\{Ni(piv)_3(bpy)\}_2Ln(NO_3)]\cdot MeCN$ (Hpiv = pivalic acid, bpy = 2,2′-bipyridine, Ln^{III} = Gd (**132**), Sm (**133**)) are isomorphous and contain a bent Ni-Ln-Ni moiety with angles ~153° [48]. The central Ln^{III} ion is bound to each of the terminal Ni^{II} ions through two *syn*,*syn* pivalato groups and one μ-O carboxylato oxygen which belongs to a chelate-monodentate bridging pivalato group. The distorted octahedral coordination around each Ni^{II} ion consists of four carboxylato oxygen atoms and two nitrogen atoms of the bpy. The magnetic susceptibility data of **132** were interpreted by using the spin Hamiltonian $H = -2J_{NiGd}(S_{Ni1}S_{Gd} + S_{Ni2}S_{Gd}) - 2J_{NiNi}(S_{Ni1}S_{Ni2})$. The best fit yielded J_{NiGd} = 0.105(5) cm^{-1}, J_{NiNi} = −0.70(5) cm^{-1}, g_{Ni} = 2.015(1), g_{Gd} = 2.00 (fixed), tip = 0.0001 ($R^2 = 1.28 \times 10^{-5}$). The neutral trinuclear complexes $[\{Ni(piv)_3(Hpiv)(MeCN)\}_2Ln(NO_3)]$ (Ln^{III} = La, Pr, Sm, Eu, Gd, **134**–**138**) [48] are isomorphous and contain a Ni-Ln-Ni moiety with angles ~144°. The central Ln^{III} ion is bound to each of the terminal Ni^{II} ions in similar fashion as in **134**–**138**. The coordination of each Ni^{II} ion is completed by a monodentate Hpiv and MeCN molecules and is distorted octahedral. The coordination of the central Ln^{III} consists of six carboxylato oxygen atoms and one chelate nitrato group and is described as single-capped pentagonal bipyramid. The magnetic susceptibility data of **138** were interpreted by using the spin Hamiltonian $H = -2J_{NiGd}(S_{Ni1}S_{Gd} + S_{Ni2}S_{Gd}) - 2J_{NiNi}(S_{Ni1}S_{Ni2})$. The best fit yielded J_{NiGd} = 0.44(2) cm^{-1}, J_{NiNi} = −2.25(5) cm^{-1}, $g_{Ni} = g_{Gd}$ = 2.00 (fixed), molar content of the S = 1 impurity is 5.5% ($R^2 = 1.5 \times 10^{-4}$). The magnetic susceptibility data of **134** can be interpreted by using either the exchange Hamiltonian $H_{ex} = -2J_{ex}S_1S_2$ which yields J_{ex} = −1.0(3) cm^{-1}, g = 2.24(1) and zJ' = +0.9(1) cm^{-1}, tip = 2.4(9) × 10^{-4} ($R^2 = 2.6 \times 10^{-4}$) or by considering the zero-field splitting of the Ni^{II} ions $H_{zfs} = D\left[S_z^2 - \left(\frac{1}{3}\right)S(S+1)\right]$ which yields D = 6.0(5) cm^{-1}, g = 2.227(1), zJ' = +0.05(1) cm^{-1}, tip = 3.6(5) × 10^{-4} ($R^2 = 2.5 \times 10^{-3}$). The magnetic susceptibility data for **135–137** which contain Pr^{III}, Sm^{III} and Eu^{III} ions can be interpreted by assuming that the exchange interactions between Ni^{II} and Ln^{III} ions are absent, whereas the weak antiferromagnetic interactions between the Ni^{II} ions 'through the lanthanide' do exist.

The ligands HL^{27} = (*Z*)-1-(pyridine-2-yl)ethenone oxime and HL^{28} = (*E*)-*N*′-hydroxypyrimidine-2-carboximidamide (Scheme 3) gave the trinuclear complexes $[\{Ni(L^{27})_3\}_2Tb](NO_3)$ (**139**) [10,11] and $[(Ni(HL^{28})_3\}_2Tb](NO_3)$ (**140**) [49], respectively. Both complexes contain strictly linear Ni-Tb-Ni moiety (Figure 14 and Figure S15). Each of the terminal Ni^{II} ions in **139**–**140** is coordinated to three pyridine and three oximato nitrogen atoms from three $(HL^{27})^-$ or $(HL^{28})^-$ ligands in distorted octahedral geometry. The central Tb^{III} ion is coordinated to six oximato oxygen atoms from the three $(HL^{27})^-$ or $(HL^{28})^-$ ligands (Scheme 3) in distorted octahedral geometry. The $\chi_M T$ values of **139** at 300 and 2 K are 13.54 and 2.80 cm^3 K mol^{-1}, respectively. The field dependence of the magnetization at 2 K is 6.41 $N\mu_B$ at 2 K. The $\chi_M T$ value of **140** at 300 K is 11.74 cm^3 K mol^{-1} which is slightly low with respect to the expected value for two Ni^{II} (S = 1) and one Tb^{III} (S = 3, L = 3, g = 3/2) non-interacting ions. The $\chi_M T$ value decreases on lowering the temperature and reaches the value of 5.41 cm^3 K mol^{-1} at 5 K. The decrease of the $\chi_M T$ value as the temperature decreases for **139** and **140** is governed by the thermal depopulation of the ground-state sublevels as result of the spin-orbit coupling and the low symmetry crystal field.

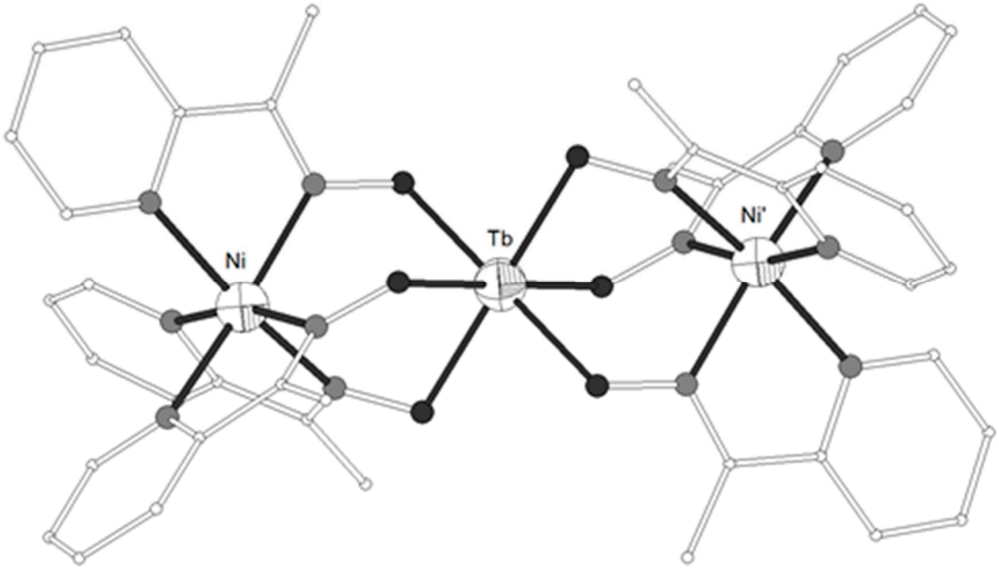

Figure 14. The molecular structure of the cation complex $[\{Ni(L^{27})_3\}_2Tb]^+$ **139**. Primed atoms are generated by symmetry: (′) $-x + y, -x, z$. Color code: Tb large octant, Ni small octant, N light grey, O dark grey, C open small, S open large [11].

It is well known that ligand L^{29} = di(pyridine-2-yl)methanone or di-2-pyridyl ketone (Scheme 3) can undergo nucleophilic addition on the carbonyl carbon atom to form the hemiketal and/or the *gem*-diol ligands $L^{29\prime}$ = ethoxydi(pyridine-2-yl)methanol and $L^{29\prime\prime}$ = di(pyridin-2-yl)methanediol, respectively. Both $L^{29\prime}$ and $L^{29\prime\prime}$ are formed in situ in the presence of metal ions. Complexes $[Ni_2(L^{29\prime})_3(L^{29\prime\prime})Ln(NO_3)(H_2O)](ClO_4)_2$ (Ln^{III} = Gd **141**, Tb **142**) and $[Ni_2(L^{29\prime})_4Ln(NO_3)(H_2O)][Ln(NO_3)_5](ClO_4)_2$ (Ln^{III} = Tb **143**, Dy **144**, Y **145**) consist of dications which contain triangular Ni-Ln-Ni moieties with angles ~54° (Figure 15) [50,51]. The metal ions are linked through one μ_3-O atom and three μ_2-O atoms from the ligands (Scheme 3). Each Ni^{II} ion is coordinated to three oxygen and two nitrogen atoms from three respective ligands in distorted octahedron. Each Ln^{III} ion is coordinated to N_2O_6 chromophore which consists of three carbonyl O-atoms, three pyridine N-atoms, one chelate nitrato and one terminal aqua ligands. The magnetic susceptibility data of **141** revealed $\chi_M T$ values of 12.61 and 18.63 cm^3 K mol^{-1} at 300 and 2 K respectively. The data were interpreted by using the spin Hamiltonian $H = -J\left(\hat{S}_{Gd}\cdot\hat{S}_{Ni1} + \hat{S}_{Gd}\cdot\hat{S}_{Ni2}\right) - J'\left(\hat{S}_{Ni1}\cdot\hat{S}_{Ni2}\right)$ and the best fit yielded J = +1.03(8) cm^{-1}, J' = +0.9(2) cm^{-1}, g = 2.246(1). The magnetization measurement at 2 K revealed saturation under 5 T at 12.9 μ_β, indicative of an S = 11/2 ground state with a g value larger than 2.0. The magnetic data of **143** revealed ferromagnetic exchange interactions between the metal ions. The magnetic susceptibility data of **145** which contains the diamagnetic Y^{III} ion allowed the determination of the magnetic exchange interaction between the Ni^{II} ions according to the above spin Hamiltonian by considering J = 0. The best fit gave J' = +8.0(2) cm^{-1} and g = 2.15(1).

The coordination geometry around the Ni^{II} ions in complexes **1**–**145** is distorted octahedral; the only exceptions are complexes **12**–**15** which can be more acutely described as trigonal prismatic. The bridging modes and the coordination around the Ni^{II} ions observed in complexes **1**–**145** is depicted in Scheme 4. The Ni^{II} ions is complexes **1**–**28**, **52**–**74**, **98**–**101** and **141**–**145** are coordinated to three nitrogen and three oxygen atoms. The configuration around the Ni^{II} ions consisting of N_3O_3 coordination sphere is chiral with either a Δ or a Λ configuration due to the screw coordination arrangement of the achiral tripodal ligands around the metal ion. When two chiral molecules associate, both homochiral (Δ-Δ or Λ-Λ) and heterochiral (Δ-Λ) pairs are possible. Since the above complexes crystallize in centrosymmetric space groups, molecules with Δ-Δ and Λ-Λ pairs coexist in the crystals to form racemic crystals. The Ni^{II} ions in complexes **29**–**51**, **75**–**83**, **91**–**93** and **109**–**131** are coordinated

to four nitrogen and two oxygen atoms. The Ni^{II} ions in **89–90** and **132–138** are coordinated to two nitrogen and four oxygen atoms and in **94–97** are coordinated to five nitrogen and one oxygen atoms. The Ni^{II} ions in **102–108** and **139–140** show N_6 coordination sphere. On the other hand, the coordination around the Ln^{III} ions in **1–145** displays a variety of geometries from the rare octahedral and quasi trigonal prism for O_6 coordination, capped trigonal prism and capped octahedron for O_7 coordination, square antiprism and bicapped octahedron for O_8 and NO_7 coordination, tricapped trigonal prism for O_9 coordination and distorted icosahedron for O_{12} coordination.

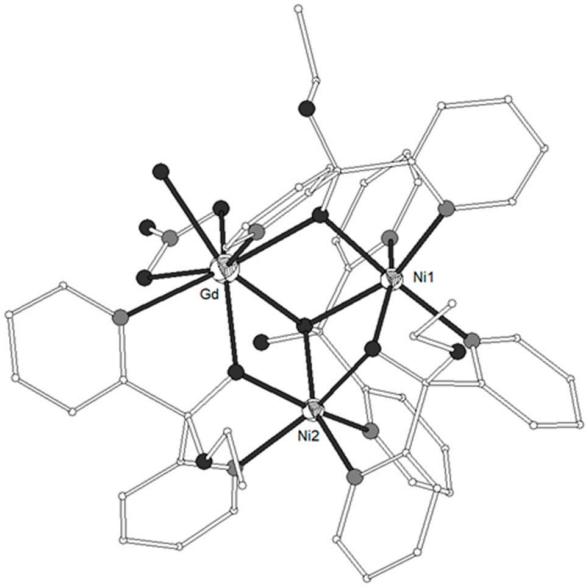

Figure 15. The molecular structure of the dication complex $[Ni_2(L^{29\prime})_3(L^{29\prime\prime})Gd(NO_3)(H_2O)]^{2+}$ **141**. Color code: Gd large octant, Ni small octant, N light grey, O dark grey, C open small, S open large [50,51].

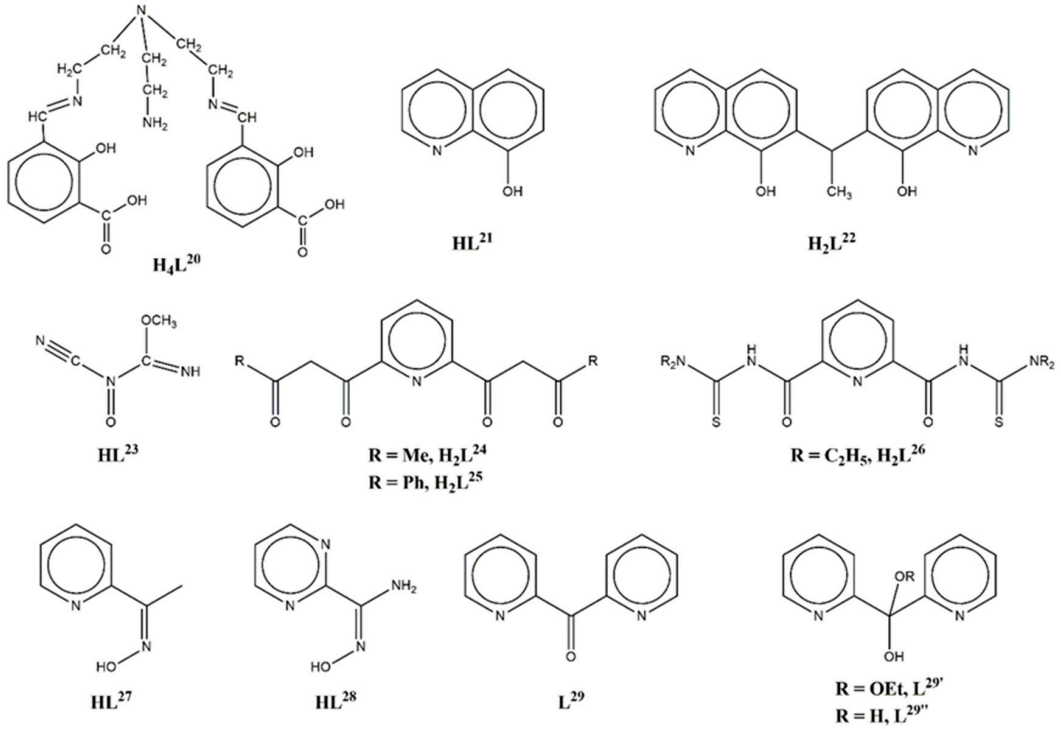

Scheme 3. The ligands used in the Ni_2Ln complexes **94–145**.

2.2. Oligonuclear Complexes Containing the Ni^{II}-Ln^{III}-Ni^{II} unit

The Schiff base ligand H_2L^{30} = 6,6′-((1*E*,1′*E*)-(propane-1,3-diylbis(azanylylidene)) bis(methanylylidene))bis(2-methoxyphenol) which resulted from the 2:1 condensation of 3-methoxysalicylaldehyde with 1,3-propanediamine (Scheme 4) gave complex [{{($NiL^{30}(H_2O)$)($N(CN)_2$)}$_2$Pr}$_2$(μ-NO_3)](OH) (**146**) [52] which consists of an hexanuclear cationic moiety built up by two almost linear Ni_2Pr subunits (Ni-Pr-Ni = 175.7°) that are linked by a disordered nitrato group bridging the two Pr^{III} ions (Figure 16). Within each Ni_2Pr subunit, the metal ions are bridged by two phenolato oxygen atoms from ligand $(L^{30})^{2-}$. Each Ni^{II} ion is also coordinated to two imino nitrogen atoms form $(L^{30})^{2-}$, one nitrogen atom from a monodentate dicyamido ligand and one aqua ligand in distorted octahedral geometry. The two Pr^{III} ions present nine- or ten-coordination (depending on the nitrato ligand coordination, monodentate or chelating) and is completed by four phenoxo and four methoxy oxygen atoms from the two $(L^{30})^{2-}$ ligands. The $\chi_M T$ product at room temperature (7.18 cm^3 K mol^{-1}) corresponds to the theoretical value for uncoupled metal ions and decreases by lowering the temperature. The susceptibility data obey the Curie-Weiss law with negative Weiss constant θ = −5.01 K and Curie constant 7.34 cm^3 K mol^{-1}.

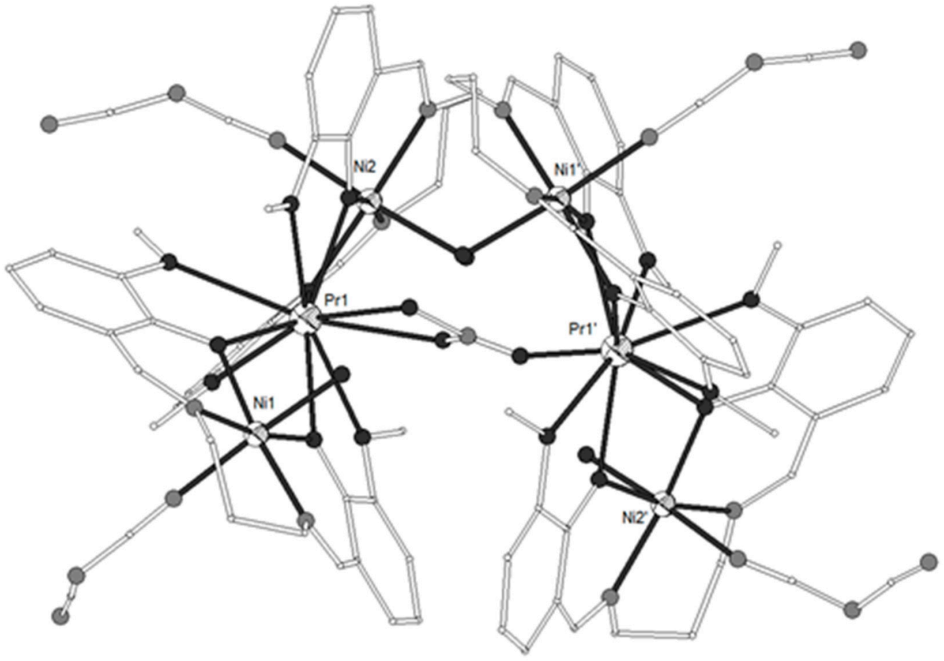

Figure 16. The molecular structure of the cationic complex [{{($NiL^{30}(H_2O)$)($N(CN)_2$)}$_2$Pr}$_2$(μ-NO_3)]$^+$ (**146**). Primed atoms are generated by symmetry (′) 1 − *x*, *y*, 0.5 − *z*. Color code: Pr large octant, Ni small octant, N light grey, O dark grey, C open small [52].

Ligand H_2L^{24} (Scheme 3) was used to prepare the hexanuclear complex [{$Ni_2(L^{24})$ $Gd(H_2O)_4$}$_2$(C_2O_4)$_3$] (**147**) which is built by two almost linear Ni_2Gd subunits (Ni-Gd-Ni = 178.6°) bridged by an oxalate ligand coordinated to the Gd^{III} ions (Figure 17) [53]. The Ni^{II} ions are hosted into the 1,3-diketonate compartments of the two ligands, in O_6 octahedral coordination completed by two aqua ligands. Each Gd^{III} ion is coordinated to the O,N,O donor atoms of the inner pocket of two ligands and two oxalate ligands, one terminal and one bridging.

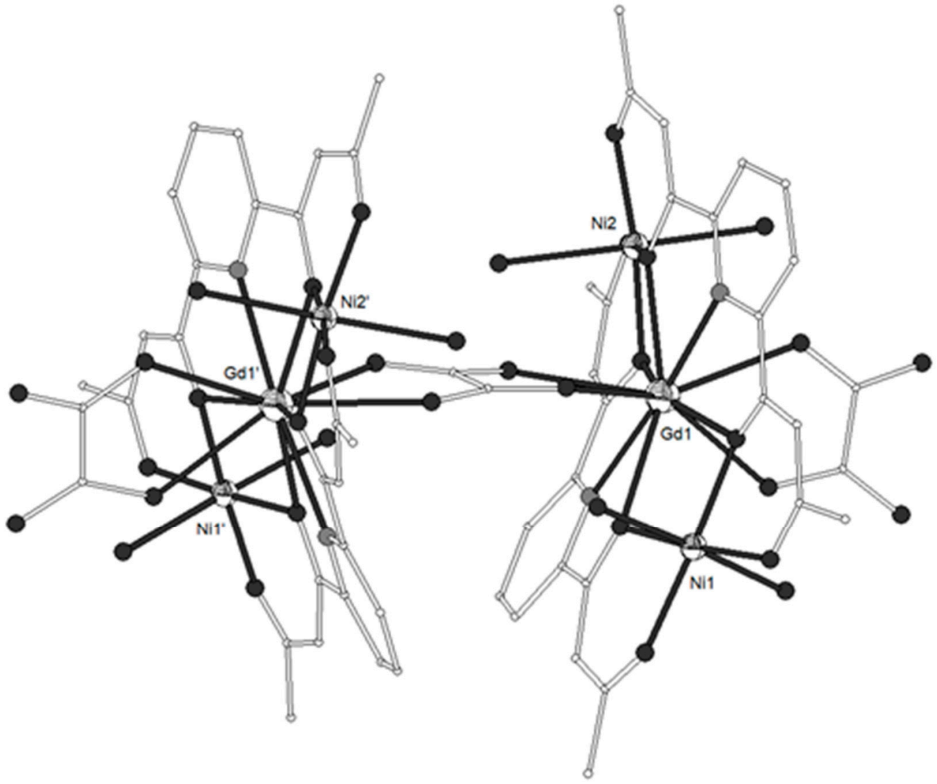

Figure 17. The molecular structure of complex $[\{Ni_2(L^{24})Gd(H_2O)_4\}_2(C_2O_4)_3]$ (**147**). Primed atoms are generated by symmetry (') $-1 - x, y, -0.5 - z$. Color code: Gd large octant, Ni small octant, N light grey, O dark grey, C open small [53].

The Schiff base ligand H_2L^{19} (Scheme 2) was used in complex $[\{Ni(L^{19})_2\}_2Dy(H_2O)Fe(CN)_6]_2$ (**148**) which consists of two almost linear Ni_2Dy subunits (Ni-Dy-Ni = 179.1°) bridged through two $[Fe(CN)_6]^{3-}$ moieties via the cyanido ligands bound to the Ni^{II} ions (Figure 18) [54]. The Ni^{II} ions are five-coordinate with the N_2O_2 donor set from one $(L^{19})^{2-}$ in the equatorial plane and the cyano nitrogen atom in the apical position of the square pyramid. Each $[Fe(CN)_6]^{3-}$ uses two *cis*-cyano ligands to coordinate to two Ni^{II} ions and is distorted octahedral. The Dy^{III} ions are bridged with each Ni^{II} ion in the Ni_2Dy subunits through two phenolato oxygen atoms and present O_9 coordination (four phenolato and four methoxy oxygen atoms from two $(L^{19})^{2-}$ and one aqua ligand) which is close to a muffin (MFF-9) or a spherical-capped square antiprism (CSAPR-9). The magnetic susceptibility measurements revealed overall ferromagnetic interactions with the $\chi_M T$ values at room temperature close to the theoretical values for four high-spin Ni^{II} ($S = 1$), two Dy^{III} ($^6H_{15/2}$) and two low-spin Fe^{III} ($S = 1/2$) ions. The field dependence of magnetization reaches a value of 25.8 Nβ at 5 T without reaching saturation probably due to the zero-field splitting effect. The complex shows a strong frequency dependence of the out-of-phase signals under zero dc field. The fitting of the $\ln(\tau)$ *vs* $1/T$ according to the Arrhenius law $\tau = \tau_0 \exp\left(\frac{\Delta}{kT}\right)$ yielded $\tau_0 = 1.6 \times 10^{-7}$ s and an effective energy barrier of $\Delta = 25.0$ K.

The ligand H_2L^{19} was also used to prepare a series of isostructural heterotrimetallic octanuclear complexes, $[(Ni(L^{19})_2\}_2Ln(H_2O)Cr(CN)_6]_2$ (Ln^{III} = Y, Gd, Tb, Dy, **149**–**153**), $[(Ni(L^{19})_2\}_2Ln(H_2O)Fe(CN)_6]_2$ (Ln^{III} = Y, Gd, Tb, **154**–**156**) and $[(Ni(L^{19})_2\}_2Ln(H_2O)Co(CN)_6]_2$ (Ln^{III} = Dy, **157**) [55]. The crystal structures of **149**–**157** are similar to that of **148** described above. Complexes **152** and **153** contain the same $[Ni_4Dy_2Cr_2]$ cyclic complex, however **153** contains also PPPO lattice molecules (PPPO = 4-(3-phenylpropyl)pyridine-1-oxide) and displays different lattice structure. The $\chi_M T$ values for **149**–**157** at 300 K are close to the theoretical values for $[Ni_4Ln_2Cr_2]$, $[Ni_4Ln_2Fe_2]$ and $[Ni_4Ln_2]$ systems of uncoupled atoms. The magnetic susceptibility data for the two $[Ni_4Y_2M_2]$

complexes (M^{III} = Cr **149**, Fe **154**) indicate the presence of ferromagnetic interactions which can be analyzed by using the isotropic Hamiltonian $\hat{H} = -2J_{NiM}\hat{S}_{M1}\left(\hat{S}_{Ni1} + \hat{S}_{Ni2}\right)$ (considering two Ni-M-Ni (M = Cr or Fe) units), by including zJ' for the intermolecular magnetic interaction and the zero-field splitting of Ni^{II} ions. The fitting yielded J_{NiCr} = 9.4(1) cm^{-1}, zJ' = −0.050(2) cm^{-1}, g = 2.06(1) for **149** and J_{NiFe} = 4.9(7) cm^{-1}, zJ' = −0.35(2) cm^{-1}, g = 2.24(1) for **154**. The positive J_{NiCr} and J_{NiFe} confirm the presence of ferromagnetic interaction between the cyanido-bridged Fe^{III}/Cr^{III} and Ni^{II} ions, whilst the negative zJ' values suggest weak antiferromagnetic interaction between the Ni-M-Ni units. The magnetic susceptibility data of the $[Ni_4Gd_2M_2]$ complexes (M^{III} = Cr **150**, Fe **155**) were fitted according the isotropic Hamiltonian $\hat{H} = -2J_{NiGd}\hat{S}_{Ni1}\hat{S}_{Gd1} - 2J_{NiGd}\hat{S}_{Ni2}\hat{S}_{Gd1} - 2J_{MNi}\hat{S}_{M1}\hat{S}_{Ni2} - 2J_{MNi}\hat{S}_{M1}\hat{S}_{Ni1A} - 2J_{NiGd}\hat{S}_{Ni1A}\hat{S}_{Gd1A} - 2J_{NiGd}\hat{S}_{Ni2A}\hat{S}_{Gd1A} - 2J_{MNi}\hat{S}_{M1A}\hat{S}_{Ni2A} - 2J_{MNi}\hat{S}_{M1A}\hat{S}_{Ni1}$ (M^{III} = Cr with S = 3/2 or Fe with S =1/2). The fitting yielded J_{NiCr} = 11.82 cm^{-1}, J_{NiGd} = 0.94 cm^{-1} and g = 2.04 for **150** and J_{NiFe} = 10.58 cm^{-1}, J_{NiGd} = 1.24 cm^{-1} and g = 2.03 for **155**. The magnetic susceptibility data of the $[Ni_4Tb_2M_2]$ (M^{III} = Cr **151** or Fe **156**) and $[Ni_4Dy_2M_2]$ (M^{III} = Cr **152**–**153** or Co **157**) complexes reveal the presence of ferromagnetic interactions. The decrease of the $\chi_M T$ values at low temperatures may be due to the zero-field splitting of Tb^{III} and Dy^{III} ions and/or the intermolecular antiferromagnetic interaction. Complexes **151**–**153** and **156**–**157** display strong frequency dependence of the out-of-phase signal below 5 K under zero dc field, indicating the presence of slow magnetic relaxation. The fitting of the $\ln(\tau)$ *vs* $1/T$ according to the Arrhenius law $\tau = \tau_0 \exp\left(\frac{U_{eff}}{kT}\right)$ yielded U_{eff} = 21.9 K ($\tau_0 = 4.71 \times 10^{-8}$ s) for **151**, U_{eff} = 38.9 K ($\tau_0 = 4.89 \times 10^{-9}$ s) for **152**, U_{eff} = 37.2 K ($\tau_0 = 6.44 \times 10^{-9}$ s) for **153**, U_{eff} = 29.6 K ($\tau_0 = 4.52 \times 10^{-10}$ s) for **156** and U_{eff} = 24.4 K ($\tau_0 = 4.94 \times 10^{-7}$ s) for **157**.

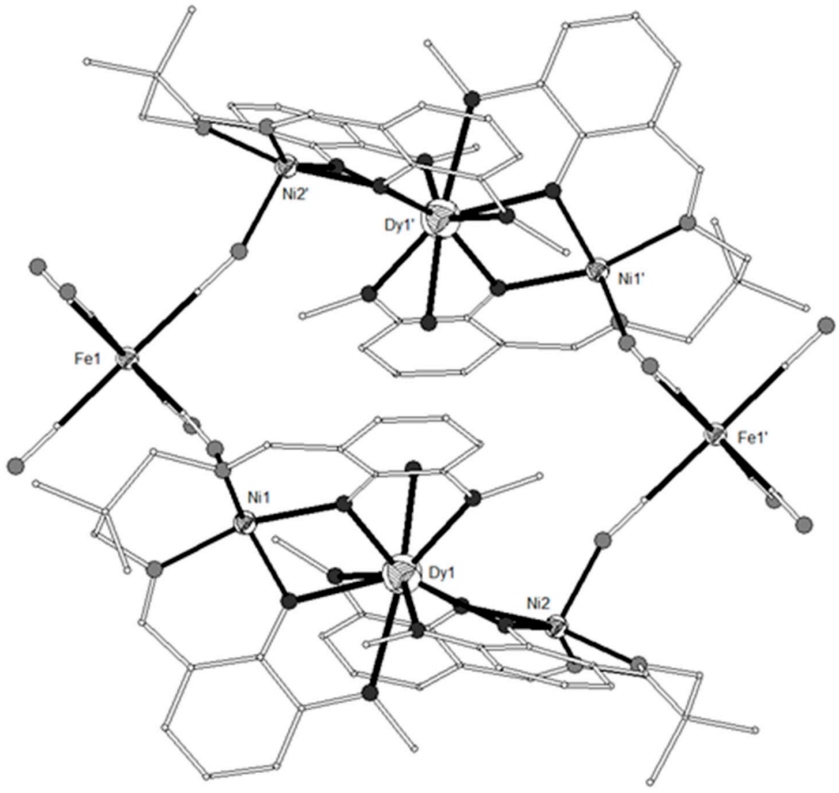

Figure 18. The molecular structure of complex $[\{Ni(L^{19})_2\}_2Dy(H_2O)Fe(CN)_6]_2$ (**148**). Primed atoms are generated by symmetry (′) 2 − x, 1 − y, 1 − z. Color code: Dy large octant, Ni and Fe small octant, N light grey, O dark grey, C open small [54].

The ligand H_2L^{19} also gave the isostructural heterotrimetallic octanuclear complexes, $[(Ni(L^{19})_2\}_2Ln(H_2O)W(CN)_8]_2$ (Ln^{III} = Tb, Dy, Y, **158**–**160**) and $[(Ni(L^{19})_2\}_2Tb(H_2O)Co(CN)_6]_2$ (**161**) [56].

The crystal structures of **158**–**161** are similar to those of complexes **148**–**157** described above; the only difference is the presence of the bridging $[W(CN)_8]^{3-}$ (**158**–**160**) or $[Co(CN)_6]^{3-}$ (**161**) moieties. The magnetic susceptibility data of **160** were fitted by using the spin Hamiltonian $H = -J(S_{Ni1}S_W + S_{Ni2}S_W)$ and including zJ' for intermolecular interaction and yielded J = 20.0(5) cm^{-1}, zJ' = −0.67(1) cm^{-1}, g_{Ni} = 2.25 and g_W = 2.0. The magnetic susceptibility data for **158** and **159** revealed ferromagnetic interactions with $\chi_M T$ values of 29.8 and 35.0 cm^3 K mol^{-1} at 300 K, 34.3 and 38.1 cm^3 K mol^{-1} at 15 K and 13 K, 8.97 and 22.4 cm^3 K mol^{-1} at 2 K. Ac-susceptibility measurements for **158** and **159** under zero dc field showed frequency dependence of the χ_M" component. Analysis of the Cole-Cole plots yielded α parameters in the narrow range 0.05–0.15 for temperatures 3–5 K which indicate very narrow distribution width of the relaxation time and a single relaxation pathway. The fitting of the $\ln(\tau)$ *vs* $1/T$ according to the Arrhenius law $\tau = \tau_0 \exp\left(\frac{U_{eff}}{kT}\right)$ yielded U_{eff} = 23.0 K ($\tau_0 = 2.57 \times 10^{-7}$ s) for **158** and U_{eff} = 26.4 K ($\tau_0 = 6.0 \times 10^{-8}$ s) for **159**. The magnetic behavior of **161** is consistent with ferromagnetic Ni-Tb interactions, however no signal for χ_M" down to 2 K under zero dc field is observed. This difference in the ac-susceptibility data between **158**–**159** and **161** is attributed to the magnetic interactions between the transition metal ions, that is, the two Ni_2W moieties for **158**–**159**, in contrast to the presence of the diamagnetic Co^{III} ions in **161**. For **158** and **161** the magnetic anisotropy is provided by the Ni^{II} and Tb^{III} ions which have identical geometry in both complexes (i.e., square pyramidal and distorted tricapped trigonal prismatic, respectively). Therefore, any effect due to modification of the Tb^{III} geometry can be ruled out and similar relaxation features are expected. However, an energy barrier of 23 K is reached for **158** whereas for **161** the slow dynamic features are very similar to those of dinuclear NiLn or trinuclear Ni_2Ln complexes.

2.3. Coordination Polymers Containing Ni^{II}-Ln^{III}-Ni^{II} Subunits

2.3.1. 1D Coordination Polymers

The ligand H_2L^{31} = 2,2′-((1*E*,1′*E*)-(propane-1,3-diylbis(axanylylidene))bis(methan ylylidene)) diphenol (Scheme 4) was used to prepare complexes $[\{(NiL^{31})_2Ln(NO_3)_3\}pyz]_n$ (pyz = pyrazine, Ln^{III} = Gd, Tb, Dy, **162**–**164**) [57]. The structure of **164** consists of $\{(NiL^{31})_2Dy(NO_3)_3\}$ subunits linked through pyrazine molecules and result in polymeric chains parallel to the (1–10) crystallographic plane (Figure 19). The asymmetric unit contains two trinuclear units with slightly different structural characteristics. The central Dy^{III} of the Ni_2Ln moiety is linked to each of the terminal Ni^{II} ions through two phenolato oxygen atoms of the $(L^{31})^{2-}$ ligand and two nitrato bridges, each one adopting different coordination mode (i.e., chelate bindentate and $\mu_{1,3}$-bridging). A third chelate nitrato ligand completes nine-coordination around the Dy^{III} ion which is described as distorted monocapped square antiprism. The two Ni^{II} ions of the Ni_2Dy moiety are hosted in the N_2O_2 pocket of the $(L^{31})^{2-}$ ligand and display distorted octahedral geometry which is completed by one nitrogen atom of the bridging pyrazine and one oxygen atom from bridging nitrato groups. The Ni-Dy-Ni moiety deviates from linearity with angles 149.6 and 153.5° for the two crystallographically independent units. The magnetic susceptibility data of **162** revealed the presence of ferromagnetic interactions between the two Ni^{II} and one Gd^{III} ions. The data were fitted by using the spin Hamiltonian $\hat{H} = -2J\hat{S}_{Gd}\left(\hat{S}_{Ni1} + \hat{S}_{Ni2}\right)$, considering $J_{GdNi1} = J_{GdNi2} = J$ and yielded $2J$ = +0.124 cm^{-1} and g = 2.044(1). The $\chi_M T$ values at 300 K for **163** and **164** are 14.4 and 16.8 cm^3 K mol^{-1}, close to the theoretical values for uncoupled one Ln^{III} and two Ni^{II} ions. The $\chi_M T$ values decrease upon lowering the temperature and reach 7.35 and 11.5 cm^3 K mol^{-1} at 2 K for **162** and **163**, respectively. The behavior of **163** and **164** can be attributed to the depopulation of the Stark sublevels of the Ln^{III} ions, the presence of zero-field splitting of the Ni^{II} ions and the exchange coupling between the metal ions. Ac magnetic susceptibility measurements for **163** and **164** did not show any signal for χ_M" under zero or 2000 Oe dc field down to 2 K.

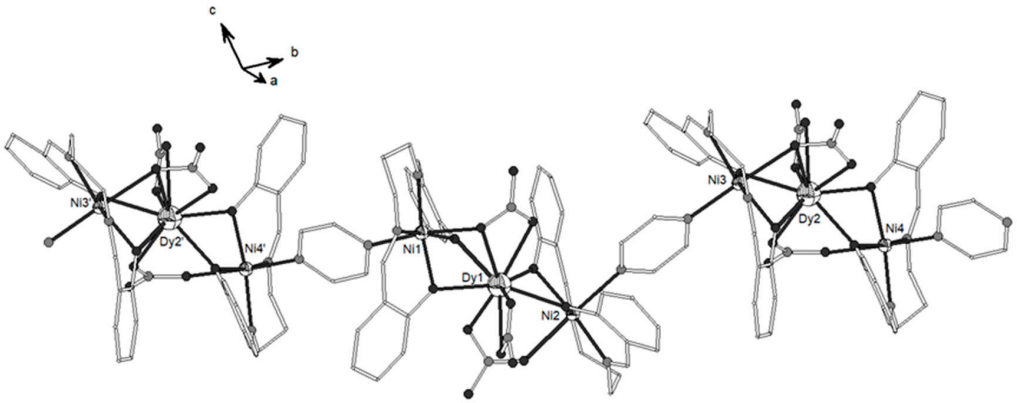

Figure 19. Part of the 1D structure of **164**. Primed atoms are generated by symmetry (′) −1 + *x*, −1 + *y*, *z*. Color code: Ln large octant, Ni small octant, N light grey, O dark grey, C open small [57].

The ligand H_2L^{24} (Scheme 3) was used to synthesize the 1D helical chain complex $[\{(NiL^{24})_2Dy(H_2O)_4(oxy\text{-}bbz)\}(NO_3)]_n$ **165** (oxy-bbz = the dianion of 4,4′-oxy-bis(benzoic) acid) [58]. The molecular structure of **165** consists of trinuclear subunits $\{Ni(L^{24})_2Dy(H_2O)_4\}^{3+}$ which are bridged through the $(oxy\text{-}bbz)^{2-}$ molecules and form cationic chains which are balanced by uncoordinated nitrate counterions (Figure 20). The helical chains of **165** extend along the crystallographic *b* axis. Each of the Ni^{II} ions is accommodated in the outer 1,3-diketone pockets of two ligands and complete distorted octahedral geometry with two aqua ligands. The central Dy^{III} ion is coordinated to the middle compartment of the two ligands and complete N_2O_8 coordination by two bidentate carboxylate groups of two different $(oxy\text{-}bbz)^{2-}$ molecules.

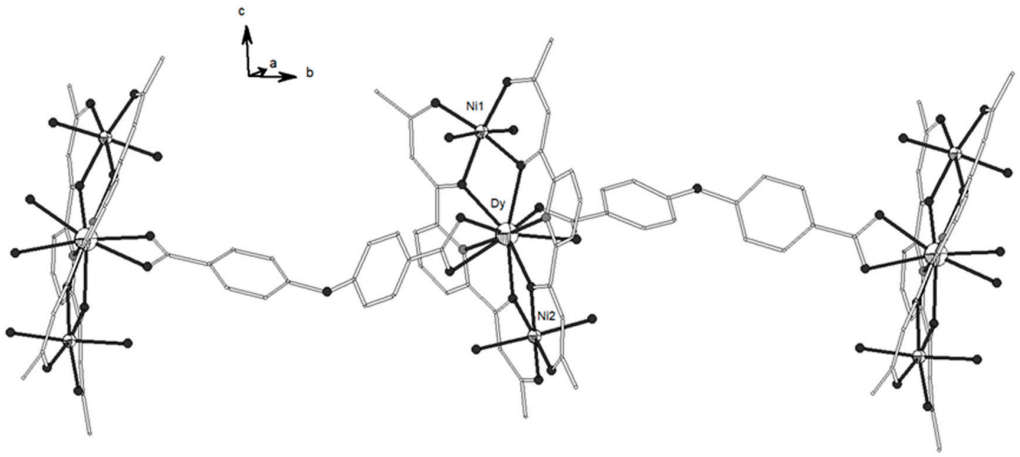

Figure 20. Part of the 1D structure of **165**. Color code as in Figure 19 [58].

Complex $Na_2[Ni(L^{32})_{1.5}]_2$ which contains the dianion of ligand H_2L^{32} = 1,3-bis(pyrazine-2-carboxamide) benzene (Scheme 4) was used as building block to afford the 1D complexes $[\{[Ni(L^{32})_{1.5}]_2Tb(H_2O)_5\}(CF_3SO_3)]_n$ (**166**) and $[\{[Ni(L^{32})_{1.5})]_2Ln(H_2O)_4(NO_3)]_n$ (Ln^{III} = Gd, Tb, **167**, **168**) [59]. The structure of **166** consists of cationic chains extending along the [101] direction of the crystal. The Tb^{III} ions link two dinuclear $[Ni(L^{32})_{1.5}]_2^{2-}$ units through coordination to one of the amidate groups of two different $(L^{32})^{2-}$ ligands with angle Ni(1)-Tb(1)-Ni(2′) = 96.7° (Figure 21). The TbO_7 coordination is completed by five aqua ligands, showing coordination polyhedron intermediate between pentagonal bipyramid (PBPY-7), capped trigonal prism (CTPR-7) and capped octahedron (COC-7). The two Ni^{II} ions exhibit distorted NiN_6 coordination environment formed by three pyrazine and three amidate nitrogen atoms in a *fac* disposition. Compounds **167** and

168 are isostructural and consist of neutral chains (Figure S16). The main difference with the cationic chains in **166** is that in the former the Ln^{III} ions are bound to a chelate NO_3^- leading to neutral chains and TbO_8 coordination described as trigonal dodecahedron (TDD-8). The Ni(1′)-Ln-Ni(2) angles are ~99.3 °. The $\chi_M T$ products of **166**–**168** at r.t. are close to the expected values for two uncoupled Ni^{II} ions ($S = 1$, $g = 2$) and one Ln^{III} ion and remain constant down to approximately 20 K and then increase sharply down to 2 K, confirming ferromagnetic exchange between the Ni^{II} and Ln^{III} ions along the chains. Complexes **166** and **168** do not show out-of-phase signals above 2 K in spite of the ferromagnetic interactions along the chains and the magnetic anisotropy of the Tb^{III} ions.

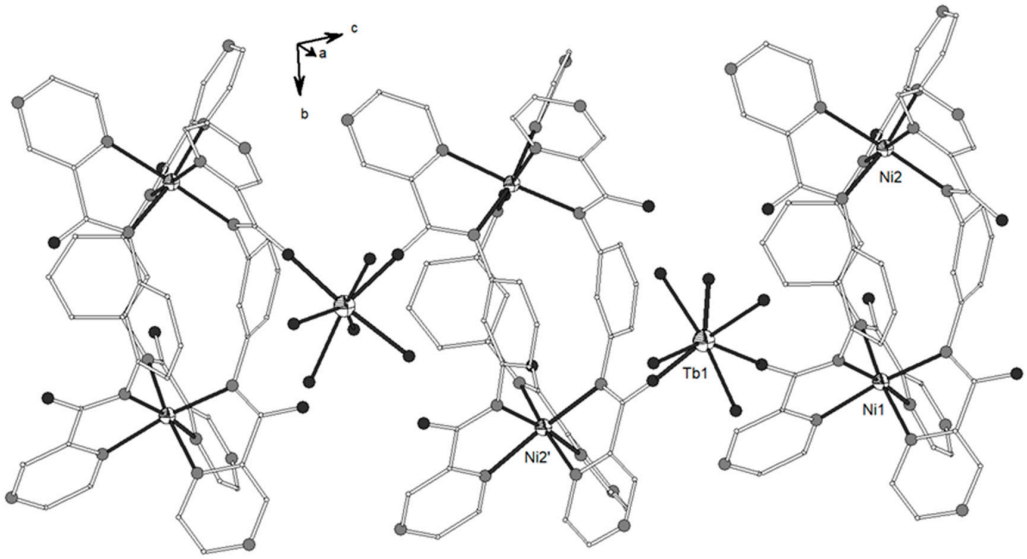

Figure 21. Part of the 1D cationic structure of **166**. Primed atom is generated by symmetry (′) $-0.5 + x$, $0.5 - y$, $-0.5 + z$. Color code as in Figure 19 [59].

The ligand H_2L^{33} = 1,3-bis(pyridine-2-carboxamide)benzene (Scheme 4) gave the cationic chains $[\{[Ni(L^{33})_{1.5}]_2Tb(H_2O)_5\}(NO_3)]_n$ (**169**) and $[\{[Ni(L^{33})_{1.5}]_2Ln(H_2O)_6\}(CF_3SO_3)]_n$ (Ln^{III} = Tb, Dy, Gd, **170**–**172**) [60]. The structure of **169** consists of cationic chains $\{[Ni(L^{33})_{1.5}]_2Tb(H_2O)_5\}^+$ extending along the (101) direction and is quite similar to the structure of **166** described above. The TbO_7 coordination sphere is a pentagonal bipyramid. The Ni(1)-Tb-Ni(2′) (′ = $-0.5 + x$, $0.5 - y$, $-0.5 + z$) angle is 99.8°. The structures of **170**–**172** consist of cationic chains $[\{[Ni(L^{33})_{1.5}]_2Ln(H_2O)_6\}^+$ and are similar to the structures of **166** and **169**. The Ln^{III} ions in **170**–**172** exhibit LnO_8 coordination environment with dodecahedral geometry and Ni1-Ln-Ni2 angles of ~73°. It should be mentioned that the Ln^{III} coordination number in **169**–**172** seems to depend on the counteranion present in the structure; TbO_7 *vs*. TbO_8 for nitrates and triflates, respectively. This has an impact on the crystal field potentials which has a direct influence on the depopulation of the Stark sublevels, the magnetic anisotropy and the magnetic properties. Compounds **169**–**171** do not exhibit magnetic slow relaxation despite the large anisotropy of the Tb^{III} and Dy^{III} ions and the existence of ferromagnetic interactions along the chains, mainly due to the weakness of the intrachain magnetic interactions.

The ligand H_4L^{34} = (13Z,19Z)-bis(2-(2-hydroxyethoxy)ethyl) 6,7-dioxo-5,6,7,8,14a,15,16,17,18,18a-decahydrotribenzo[b,f,l] [1,4,8,11] tetraazacyclotetradecin e-13,20-dicarboxylate (Scheme 4) gave three isomorphous double-chain coordination polymers $[\{(Ni(H_2L^{34}))_2Ln(H_2O)_3\}(ClO_4)_3]_n$ (Ln^{III} = Pr, Sm, Gd, **173**–**175**, Figure 22) which contain the repeating unit $[\{(Ni(H^2L^{34}))_2Ln(H_2O)_3\}^{3+}$ with almost linear Ni^{II}-Ln^{III}-Ni^{II} moieties (~179.3°) [61]. The coordination mode of the $(H_2L^{34})^{2-}$ ligands promotes the formation of rectangular $Ln_2(Ni(H_2L^{34}))_2$ subunits. Both Ni^{II} ions present slightly distorted N_4 square planar coordination geometry. The central Ln^{III} ion presents O_9 coordination defined from two bidentate oxamido groups belonging to two different $(H_2L^{34})^{2-}$, two hydroxyls belonging to two

different $(H_2L^{34})^{2-}$ and three aqua ligands. The coordination geometry around the Ln^{III} ion is described as distorted monocapped square antiprism. Compounds **173**–**175** were able to induce DNA cleavage.

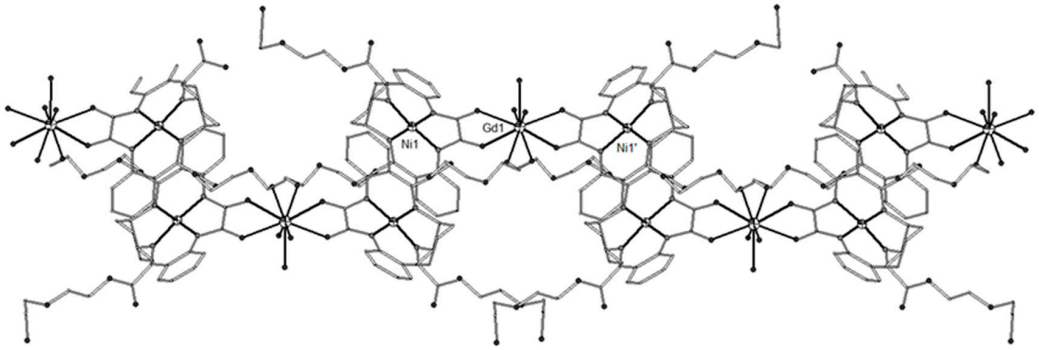

Figure 22. Part of the double-chain structure of **175**. Primed atom is generated by symmetry (′) $1 - x$, y, $1.5 - z$. Color code as in Figure 19 [61].

The Schiff base ligand HL^{35} obtained from the condensation of 2-pyridylaldehyde with isonicotinic hydrazide N-oxide (Scheme 4) gave three 1D polymers with formula $[\{(Ni(L^{35})_{1.5})_2Ln(HL^{35})(dmf)_4\}(ClO_4)_4]_n$ (Ln^{III} = Gd, Tb, **176**–**177**) and $[\{(Ni(L^{35})_2)_2Dy(dmf)_4\}(ClO_4)_3]_n$ (**178**) which are based on trinuclear Ni_2Ln subunits albeit consist of corner-sharing squares Ni_2Ln_2 due to the coordination mode adopted by the ligand [62].

2.3.2. 2D Coordination Polymers

The ligands H_2L^{36} = oxydiacetic acid (Scheme 4) and dpds = 4,4′-dipyridyl disulfide gave the 2D coordination polymer $[\{Ni(L^{36})_{1.5}\}_2Eu(dpds)_2(H_2O)_4]_n$ (**179**) with Ni^{II}-Eu^{III}-Ni^{II} moiety forming an angle of 145.7° [63]. The Eu^{III} ion is coordinated to three ether and six carboxylate oxygen atoms from three $(L^{36})^{2-}$ ligands and shows tricapped trigonal prismatic geometry. Each of the Ni^{II} ions is bound to two aqua ligands, two pyridyl nitrogen atoms from two dpds ligands and two carboxylate oxygen atoms from two neighboring $(L^{36})^{2-}$ ligands in distorted octahedral geometry. The $(L^{36})^{2-}$ ligands display two coordination modes, half of them behave as pentadentate ligands chelating one Eu^{III} ion and bridging two Ni^{II} ions and the other half act as tetradentate chelating one Eu^{III} ion and bridging a Ni^{II} ion. The bridging action provided by the $(L^{36})^{2-}$ and dpds ligands results in the formation of an overall 2D layer structure in (100) plane (Figure 23).

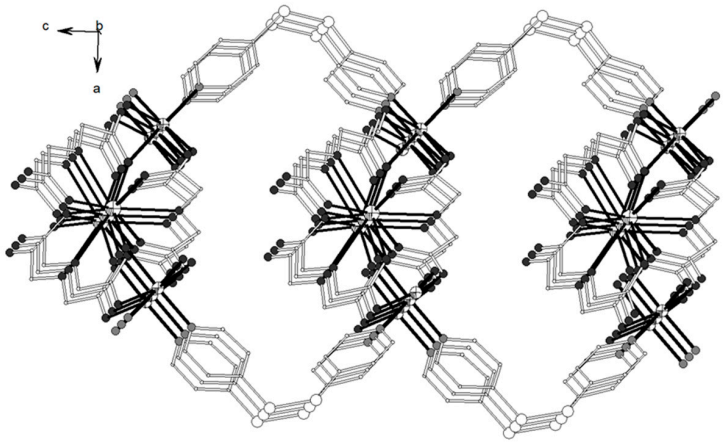

Figure 23. Part of the 2D layer structure of **179**. Color code: Eu large octant, Ni small octant, N light grey, O dark grey, C open small, S open large [63].

2.3.3. 3D Coordination Polymers

Isonicotinic acid (HL^{37}, Scheme 4) gave three 3D coordination frameworks of general formula $[\{Ni(L^{37})_{2.5}(N_3)(H_2O)\}_2Ln(H_2O)]_n$ (Ln^{III} = Gd, Pr, Nd, **180–182**) [64,65]. The structures contain one Ln^{III} and two Ni^{II} ions two unique azide ligands and five different isonicotinate anions. Th Ln^{III} ions are coordinated to nine oxygen atoms, two doubly coordinated and four singly coordinated carboxylates and one aqua ligand. The two tridentate $(L^{37})^-$ anions bridge the Ln^{III} ions into 1D zig-zag chain via the carboxylate groups and also bound to Ni(1) through the N atoms. Two alternating end-on and end-to-end azides connect the Ni(1) ions into chain which is further linked to neighboring Ln^{III} ions via μ-O,O,N $(L^{37})^-$ ligands, resulting in 2D sheets. The three bidentate $(L^{37})^-$ ligands are coordinated to Ni(2) ions and also to Ni(1) and Ln^{III} ions resulting in the formation of an overall 3D network. Magnetic susceptibility studies of **180** revealed the presence of ferrimagnetic coupling between the Ni^{II} and Gd^{III} ions and the contribution of the alternating end-on and end-to-end azido system which corresponds to an alternating ferromagnetic-antiferromagnetic chain in the temperature range 40–300 K, as well as zero-field splitting of the Ni^{II} ions in the low temperatures regime. In the case of **181–182** the magnetic susceptibility data indicate the presence of dominant antiferromagnetic interactions between the metal ions.

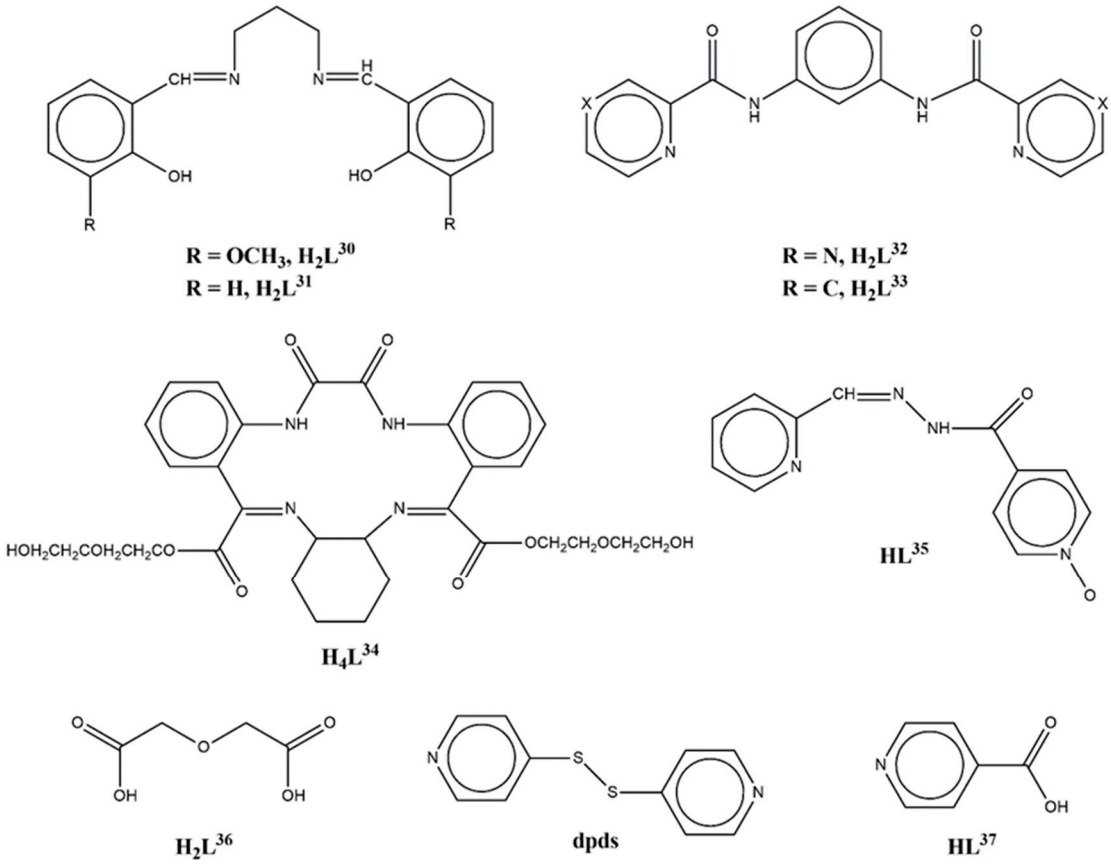

Scheme 4. Ligands used in the oligonuclear and polynuclear complexes **146–182** which contain the Ni_2Ln moiety.

3. Summary

Trinuclear heterometallic complexes containing the Ni^{II}-Ln^{III}-Ni^{II} moiety, with Ni-Ln-Ni angles in the range ~54–180°, have been reported with Ln^{III} = Y, La-Lu except Pm. In these complexes, the Ni^{II} ions display octahedral coordination geometry comprised of N_3O_3, N_2O_4, N_4O_2, N_5O, NO_5, N_6, O_6 and O_2S_4 chromophores. Rare examples containing square planar NiN_2O_2, NiN_4 and square

pyramidal NiN_2O_3, NiN_3O_2 coordination geometries have been also reported. The complexes that contain the N_3O_3 chromophore are chiral with either a Δ or a Λ configuration due to the screw coordination arrangement of the achiral ligands around the metal ion; however, the complexes reported herein crystallize in centrosymmetric space groups therefore the Δ-Δ and Λ-Λ pairs coexist in the crystals to form racemic crystals. The coordination geometry around the Ln ions range from the rare octahedral, quasi trigonal prism and trigonal antiprism for six-coordination; capped trigonal prism, capped octahedron and pentagonal bipyramid for seven-coordination; square antiprism, bicapped octahedron and single-capped pentagonal bipyramid for eight-coordination; tricapped trigonal prism and hula-hoop for nine-coordination; sphenocorna, pentagonal antiprism, tetradecahedron, hexadecahedron, dodecahedron and double-capped square antiprism for ten-coordination; and distorted icosahedron for twelve-coordination. The magnetic properties of the trinuclear complexes range from ferro- to antiferromagnetic depending on the lanthanide ion. All Ni_2Gd complexes display weak ferromagnetic interactions between the metal ions leading to ground spin state $S = 11/2$. The magnetic exchange parameters of the Ni_2Gd were found in the range +0.19 to +1.03 cm^{-1}. Some of the Ni_2Dy complexes showed zero-filed or field-induced SMM behavior with thermal barriers in the range 10–14 K and pre-exponential factors τ_0 ~10^{-5}–10^{-6} s. The trinuclear complexes were linked via inorganic and/or organic anions to form dimers of trimers. The use of bridging complex anions, such as $[M^{III}(CN)_6]^{3-}$ (M^{III} = Fe, Cr, Co) and $[W^{V}(CN)_8]^{3-}$, afforded cyclic heterometallic complexes $[Ni_2LnM]_2$ which exhibit SMM behavior under zero dc field with energy barriers in the range ~22–39 K and τ_0 ~10^{-7}–10^{-10} s. The trinuclear Ni^{II}-Ln^{III}-Ni^{II} moiety was found as the repeating unit in 1D-, 2D and 3D-coordination polymers with interesting structures and physical properties.

Supplementary Materials: The following are available online at http://www.mdpi.com/2073-4352/10/12/1117/s1, Figures S1–S16 showing the molecular structure of the complexes mentioned in the text.

Funding: This research received no external funding.

Conflicts of Interest: The author declares no conflict of interest.

References

1. Lis, T. Preparation, structure, and magnetic properties of dodecanuclear mixed-valence manganese carboxylate. *Acta Cryst.* **1980**, *36*, 2042–2046. [CrossRef]
2. Caneschi, A.; Gatteschi, D.; Sessoli, R. Alternating current susceptibility, high field magnetization, and millimeter band EPR evidence for a ground $S = 10$ state in $[Mn_{12}O_{12}(CH_3COO)_{16}(H_2O)_4]\cdot 2CH_3COOH\cdot 4H_2O$. *J. Am. Chem. Soc.* **1991**, *113*, 5873–5874. [CrossRef]
3. Sessoli, R.; Tsai, H.-L.; Schake, A.R.; Wang, S.; Vincent, J.B.; Folting, K.; Gatteschi, D.; Christou, G.; Hendrickson, D.N. High-spin molecules: $[Mn_{12}O_{12}(O_2CR)_{16}(H_2O)_4]$. *J. Am. Chem. Soc.* **1993**, *115*, 1804–1816. [CrossRef]
4. Weighardt, K.; Pohl, D.; Jibril, I.; Huttner, G. Hydrolysis products of the monomeric amine complex $(C_6H_{15}N_3)FeCl_3$: The structure of the octameric iron(III) cation of $\{[(C_6H_{15}N_3)_6Fe_8(\mu_3\text{-}O)_2(m_2\text{-}OH)_{12}]Br_7(H_2O)\}Br\cdot 8H_2O$. *Angew. Chem. Int. Ed. Engl.* **1984**, *23*, 77–78. [CrossRef]
5. Delfs, C.; Gatteschi, D.; Pardi, L.; Sessoli, R.; Weighardt, K.; Hank, D. Magnetic properties of an octanuclear iron(III) cation. *Inorg. Chem.* **1993**, *32*, 3099–3103. [CrossRef]
6. Ishikawa, N.; Sugita, M.; Ishikawa, T.; Koshihara, S.-Y.; Kaizu, Y. Lanthanide double-decker complexes functioning as magnets at the single-molecule level. *J. Am. Chem. Soc.* **2003**, *125*, 8694–8695. [CrossRef]
7. Zadrozny, J.M.; Xiao, D.J.; Atanasov, M.; Long, G.J.; Grandjean, F.; Neese, F.; Long, J.R. Magnetic blocking in a linear iron(I) complex. *Nat. Chem.* **2013**, *5*, 577–581. [CrossRef]
8. Caneschi, A.; Gatteschi, D.; Lalioti, N.; Sangregorio, C.; Sessoli, R.; Venturi, G.; Vindigni, A.; Rettori, A.; Pini, M.G.; Novak, M.A. Cobalt(II)-nitronyl nitroxide chains as molecular magnetic nanowires. *Angew. Chem. Int. Ed. Engl.* **2001**, *40*, 1760–1763. [CrossRef]

9. Lada, Z.G.; Katsoulakou, E.; Perlepes, S.P. Synthesis and Chemistry of Single-Molecule Magnets. In *Single-Molecule Magnets-Molecular Architectures and Building Blocks for Spintronics*; Holynska, M., Ed.; Wiley-VCH Verlag GmbH & Co: Weinheim, Germany, 2019.
10. Polyzou, C.D.; Efthymiou, C.G.; Escuer, A.; Cuhna-Silva, L.; Papatriantafyllopoulou, C.; Perlepes, S.P. In search of 3d/4f-metal single-molecule magnets: Nickel(II)/lanthanide(III) coordination clusters. *Pure Appl. Chem.* **2013**, *85*, 315–327. [CrossRef]
11. Papatriantafyllopoulou, C.; Estrader, M.; Efthymiou, C.G.; Dermitzaki, D.; Gkotsis, K.; Terzis, A.; Diaz, C.; Perlepes, S.P. In search for mixed transition metal/lanthanide single-molecule magnets: Synthetic routes to Ni^{II}/Tb^{III} and Ni^{II}/Dy^{III} clusters featuring a 2-pyridyl oximate ligand. *Polyhedron* **2009**, *28*, 1652–1655. [CrossRef]
12. Osa, S.; Kido, T.; Matsumoto, N.; Re, N.; Pochaba, A.; Mrozinski, J. A tetranuclear 3d-4f single molecule magnet: $[Cu^{II}LTb^{III}(hfac)_2]_2$. *J. Am. Chem. Soc.* **2004**, *126*, 420–421. [CrossRef] [PubMed]
13. Benchini, A.; Benelli, C.; Caneschi, A.; Carlin, R.L.; Dei, A.; Gatteschi, D. Crystal and molecular structure of and magnetic coupling in two complexes containing gadolinium(III) and copper(II) ions. *J. Am. Chem. Soc.* **1985**, *107*, 8128–8136. [CrossRef]
14. Costes, J.-P.; Dahan, F.; Dupuis, A.; Laurent, J.P. A genuine example of a discrete bimetallic (Cu, Gd) complex: Structural determination and magnetic properties. *Inorg. Chem.* **1996**, *35*, 2400–2402. [CrossRef] [PubMed]
15. Pasatoiu, T.D.; Sutter, J.-P.; Madalan, A.M.; Fellah, F.Z.C.; Duhayon, C.; Andruh, M. Preparation, crystal structures, and magnetic features for a series of dinuclear $[Ni^{II}Ln^{III}]$ Schiff-base complexes: Evidence for slow relaxation of the magnetization for the Dy^{III} derivative. *Inorg. Chem.* **2011**, *50*, 5890–5898. [CrossRef] [PubMed]
16. Yamaguchi, T.; Costes, J.-P.; Kishima, Y.; Kojima, M.; Sunatsuki, Y.; Bréfuel, N.; Tuchagues, J.-P.; Vendier, L.; Wernsdorfer, W. Face-sharing heterotrinuclear M^{II}-Ln^{III}-M^{II} (M = Mn, Fe, Co, Zn; Ln = La, Gd, Tb, Dy) complexes: Synthesis, structures, and magnetic properties. *Inorg. Chem.* **2010**, *49*, 9125–9135. [CrossRef] [PubMed]
17. Chandrasekhar, V.; Pandian, B.M.; Boomishankar, R.; Steiner, A.; Vittal, J.J.; Houri, A.; Clérac, R. Trinuclear heterobimetallic Ni_2Ln complexes $[L_2Ni_2Ln](ClO_4)$ (Ln = La, Ce, Pr, Nd, Sm, Eu, Gd, Tb, Dy, Ho, and Er; LH_3 = (S)P[N(Me)N=CH-C_6H_3-2-OH_3-OMe]$_3$): From simple paramagnetic complexes to single-molecule magnet behavior. *Inorg. Chem.* **2008**, *47*, 4918–4929. [CrossRef] [PubMed]
18. Singh, S.K.; Rajeshkumar, T.; Chandrasekhar, V.; Rajaraman, G. Theoretical studies on {3d-Gd} and {3d-Gd-3d} complexes: Effect of metal substitution on the effective exchange interaction. *Polyhedron* **2013**, *66*, 81–86. [CrossRef]
19. Yamaguchi, T.; Sunatsuki, Y.; Kojima, M.; Akashi, H.; Tsuchimoto, M.; Re, N.; Osa, S.; Matsumoto, N. Ferromagnetic Ni^{II}-Gd^{III} interactions in complexes with NiGd, NiGdNi, and NiGdGdNi cores supported by tripodal ligands. *Chem. Commun.* **2004**, 1048–1049. [CrossRef]
20. Yamaguchi, T.; Sunatsuki, Y.; Ishida, H.; Kajima, M.; Akashi, H.; Re, N.; Matsumoto, N.; Pochaba, A.; Mroziński, J. Synthesis, structures, and magnetic properties of double face-sharing heterotrinuclear Ni^{II}-Ln^{III}-Ni^{II} (Ln = Eu, Gd, Tb, and Dy) complexes. *Bull. Chem. Soc. Jpn.* **2008**, *81*, 598–605. [CrossRef]
21. Costes, J.-P.; Yamaguchi, T.; Kojima, M.; Vendier, L. Experimental evidence for the participation of 5d Gd^{III} orbitals in the magnetic interaction in Ni-Gd complexes. *Inorg. Chem.* **2009**, *48*, 5555–5561. [CrossRef]
22. Yao, M.-X.; Zhu, Z.-X.; Lu, X.-Y.; Deng, X.-W.; Jing, S. Rare single-molecule magnets with six-coordinate Ln^{III} ions exhibiting a trigonal antiprism configuration. *Dalton Trans.* **2016**, *45*, 10689–10695. [CrossRef] [PubMed]
23. Xu, Z.; Read, P.W.; Hibbs, D.E.; Hursthouse, M.B.; Abdul Malik, K.M.; Patrick, B.O.; Rettig, S.J.; Seid, M.; Summers, D.A.; Pink, M.; et al. Coaggregation of paramagnetic d- and f-block metal ions with a podand-framework amine phenol ligand. *Inorg. Chem.* **2000**, *39*, 508–516. [CrossRef] [PubMed]
24. Bayly, S.R.; Xu, Z.; Patrick, B.O.; Rettig, S.J.; Pink, M.; Thompson, R.C.; Orvig, C. d/f complexes with uniform coordination geometry: Structural and magnetic properties of an $LnNi_2$ core supported by a heptadentate amine phenol ligand. *Inorg. Chem.* **2003**, *42*, 1576–1583. [CrossRef] [PubMed]
25. Mustapha, A.; Reglinski, J.; Kennedy, A.R. The use of hydrogenated Schiff base ligands in the synthesis of milti-metallic compounds. *Inorg. Chim. Acta* **2009**, *362*, 1267–1274. [CrossRef]
26. Wen, H.-R.; Dong, P.-P.; Liu, S.-J.; Liao, J.-S.; Liang, F.-Y.; Liu, C.-M. 3d-4f heterometallic trinuclrear complexes derived from amine-phenol tripodal ligands exhibiting magnetic and luminescent properties. *Dalton Trans.* **2017**, *46*, 1153–1162. [CrossRef]

27. Barta, C.A.; Bayly, S.R.; Read, P.W.; Patrick, B.O.; Thompson, R.C.; Orvig, C. Molecular architectures for trimetallic d/f/d complexes: Structural and magnetic properties of a $LnNi_2$ core. *Inorg. Chem.* **2008**, *47*, 2280–2293. [CrossRef]
28. Comba, P.; Enders, M.; Großhauser, M.; Hiller, M.; Müller, D.; Wadepohl, H. Solution and solid state structures and magnetism of a series of linear trinuclear compounds with a hexacoordinate Ln^{III} and two terminal Ni^{II} centers. *Dalton Trans.* **2017**, *46*, 138–149. [CrossRef]
29. Wen, H.-R.; Zhang, J.-L.; Liang, F.-Y.; Yang, K.; Liu, S.-J.; Liao, J.-S.; Liu, C.-M. Tb^{III}/3d-Tb^{III} clusters derived from a 1,4,7-triazacyclononane-based hexadentate ligand with field-induced slow magnetic relaxation and oxygen-sensitive luminescence. *New J. Chem.* **2019**, *43*, 4067–4074. [CrossRef]
30. Upadhyay, A.; Komatireddy, N.; Ghirri, A.; Tuna, F.; Langley, S.K.; Srivastava, A.K.; Sañudo, E.C.; Moubaraki, B.; Murray, K.S.; McInnes, E.J.L.; et al. Synthesis and magnetothermal properties of a ferromagnetically coupled Ni^{II}-Gd^{III}-Ni^{II} cluster. *Dalton Trans.* **2014**, *43*, 259–266. [CrossRef]
31. Upadhyay, A.; Das, C.; Langley, S.K.; Murray, K.S.; Srivastava, A.K.; Shanmugam, M. Heteronuclear Ni(II)-Ln(III) (Ln = La, Pr, Tb, Dy) complexes: Synthesis and single-molecule magnet behavior. *Dalton Trans.* **2016**, *45*, 3616–3626. [CrossRef]
32. Ahmed, N.; Das, C.; Vaidya, S.; Kumar Srivastava, A.; Langley, S.K.; Murray, K.S.; Shanmugam, M. Probing the magnetic and magnetothermal properties of M(II)-Ln(III) complexes (where M(II) = Ni or Zn; Ln(III) = La or Pr or Gd). *Dalton Trans.* **2014**, *43*, 17375–17384. [CrossRef] [PubMed]
33. Das, S.; Dey, A.; Kundu, S.; Biswas, S.; Mota, A.J.; Colacio, E.; Chandrasekhar, V. Linear {Ni^{II}-Ln^{III}-Ni^{II}} complexes containing twisted planar Ni(μ-phenolate)$_2$Ln fragments: Synthesis, structure, and magnetothermal properties. *Chem. Asian. J.* **2014**, *9*, 1876–1887. [CrossRef] [PubMed]
34. Georgopoulou, A.N.; Pissas, M.; Psycharis, V.; Sanakis, Y.; Raptopoulou, C.P. Trinuclear Ni^{II}-Ln^{III}-Ni^{II} complexes with Schiff base ligands: Synthesis, structure, and magnetic properties. *Molecules* **2020**, *25*, 2280. [CrossRef] [PubMed]
35. Sui, Y.; Hu, R.-H.; Liu, D.-S.; Wu, Q. Adjustment of the structures and biological activities by the ratio of NiL to RE for two sets of Schiff base complexes [$(NiL)_nRE$] (n = 1 or 2; RE = La or Ce). *Inorg. Chem. Comm.* **2011**, *14*, 396–398. [CrossRef]
36. Ali Güngör, S.; Kose, M. Synthesis, crystal structure, photoluminescence and electrochemical properties of a sandwiched Ni_2Ce complex. *J. Mol. Struct.* **2017**, *1150*, 274–278. [CrossRef]
37. Cristovao, B.; Kłak, J.; Miroslaw, B. Synthesis, crystal structures and magnetic behavior of Ni^{II}-4f-Ni^{II} compounds. *Polyhedron* **2012**, *43*, 47–54. [CrossRef]
38. Cristóvão, B.; Kłak, J.; Pełka, R.; Miroslaw, B.; Hnatejko, Z. Heterometallic trinuclear 3d-4f-3d compounds based on a hexadentate Schiff base ligand. *Polyhedron* **2014**, *68*, 180–190. [CrossRef]
39. Ghosh, S.; Ghosh, A. Coordination of metalloligand [NiL] (H_2L = salen type N_2O_2 Schiff base ligand) to the f-block elements: Structural elucidation and spectrophotometric investigation. *Inorg. Chim. Acta* **2016**, *442*, 64–69. [CrossRef]
40. Costes, J.-P.; Donnadieu, B.; Gheorghe, R.; Novitchi, G.; Tuchagues, J.-P.; Vendier, L. Di- or trinuclear 3d-4f Schiff base complexes: The role of anions. *Eur. J. Inorg. Chem.* **2008**, 5235–5244. [CrossRef]
41. Bhunia, A.; Yadav, M.; Lan, Y.; Powell, A.K.; Menges, F.; Riehn, C.; Niedner-Schatteburg, G.; Jana, P.P.; Riedel, R.; Harms, K.; et al. Trinuclear nickel-lanthanide compounds. *Dalron Trans.* **2013**, *42*, 2445–2450. [CrossRef]
42. Deacon, G.B.; Forsyth, C.M.; Junk, P.C.; Leary, S.G. A rare earth alloy as a synthetic reagent: Contrasting homometallic rare earth and heterobimetallic outcomes. *New J. Chem.* **2006**, *30*, 592–596. [CrossRef]
43. Zhu, Y.; Luo, F.; Song, Y.-M.; Feng, X.-F.; Luo, M.-B.; Liao, Z.-W.; Sun, G.-M.; Tian, X.-Z.; Yuan, Z.-J. The first one-pot synthesis of multinuclear 3d-4f metal-organic compounds involving a polytopic N,O-donor ligand formed in situ. *Cryst. Growth Des.* **2012**, *12*, 2158–2161. [CrossRef]
44. Chesman, A.S.R.; Turner, D.R.; Moubaraki, B.; Murray, K.S.; Deacon, G.B.; Batten, S.R. Synthesis and magnetic properties of a series of 3d/4f/3d heterometallic trinuclear complexes incorporating in situ ligand formation. *Inorg. Chim. Acta* **2012**, *389*, 99–106. [CrossRef]
45. Shiga, T.; Ito, N.; Hidaka, A.; Okawa, H.; Kitagawa, S.; Ohba, M. A series of trinuclear $Cu^{II}Ln^{III}Cu^{II}$ complexes derived from 2,6-di(acetoacetyl)pyridine: Synthesis, structure, and magnetism. *Inorg. Chem.* **2007**, *46*, 3492–3501. [CrossRef]

46. Trieu, T.N.; Nguyen, M.H.; Abram, U.; Nguyen, H.H. Syntheses and structures of new trinuclear $M^{II}LnM^{II}$ (M = Ni, Co; Ln = Gd, Ce) complexes with 2,6-bis(acetobenzoyl)pyridine. *Z. Anorg. Allg. Chem.* **2015**, *641*, 863–870. [CrossRef]
47. Nguyen, H.H.; Jegathesh, J.J.; Takiden, A.; Hauenstein, D.; Pham, C.T.; Le, C.D.; Abram, U. 2,6-dipicolinoylbis(N,N-dialkylthioureas) as versatile building blocks for oligo- and polynuclear architectures. *Dalton Trans.* **2016**, *45*, 10771–10779. [CrossRef]
48. Burkovskaya, N.P.; Orlova, E.V.; Kiskin, M.A.; Efimov, N.N.; Bogomyakov, A.S.; Fedin, M.V.; Kolotilov, S.V.; Minin, V.V.; Aleksandrov, G.G.; Sidorov, A.A.; et al. Synhtesis, structure, and magnetic properties of heterometallic trinuclear complexes $\{M^{II}\text{-}Ln^{III}\text{-}M^{II}\}$ (M^{II} = Ni, Cu; Ln^{III} = La, Pr, Sm, Eu, Gd). *Russ. Chem. Bull Int. Ed.* **2011**, *60*, 2490–2503. [CrossRef]
49. Kalogridis, C.; Palacios, M.A.; Rodríguez-Diéguez, A.; Mota, A.J.; Choquesillo-Lazarte, D.; Brechin, E.K.; Colacio, E. Heterometallic oximato-bridged linear trinuclear $Ni^{II}\text{-}M^{III}\text{-}Ni^{II}$ (M^{III} = Mn, Fe, Tb) complexes constructed with the *fac*-O_3 $[Ni(HL)_3]^-$ metalloligand (H_2L = pyrimidine-2-carboxamide oxime): A theoretical and experimental magneto-structural study. *Eur. J. Inorg. Chem.* **2011**, 5225–5232. [CrossRef]
50. Efthymiou, C.G.; Georgopoulou, A.N.; Papatriantafyllopoulou, C.; Terzis, A.; Raptopoulou, C.P.; Escuer, A.; Perlepes, S.P. Initial employment of di-2-pyridyl ketone as a route to nickel(II)/lanthanide(III) clusters: Triangular Ni_2Ln complexes. *Dalton Trans.* **2010**, *29*, 8603–8605. [CrossRef]
51. Georgopoulou, A.N.; Efthymiou, C.G.; Papatriantafyllopoulou, C.; Psycharis, V.; Raptopoulou, C.P.; Manos, M.; Tasiopoulos, A.J.; Escuer, A.; Perlepes, S.P. Triangular $Ni^{II}{}_2Ln^{III}$ and $Ni^{II}{}_2Y^{III}$ complexes derived from di-2-pyridyl ketone: Synthesis, structures and magnetic properties. *Polyhedron* **2011**, *30*, 2978–2986. [CrossRef]
52. Gheorghe, R.; Andruh, M.; Costes, J.-P.; Donnadieu, B.; Schmidtmann, M.; Müller, A. Making 3d-4f hexanuclear clusters from heterotrinuclear cationic building blocks. *Inorg. Chim. Acta* **2007**, *360*, 4044–4050. [CrossRef]
53. Dinca, A.S.; Shova, S.; Ion, A.E.; Maxim, C.; Lloret, F.; Julve, M.; Andruh, M. Ascorbic acid decomposition into oxalate ions: A simple synthetic route towards oxalate-bridged heterometallic 3d-4f clusters. *Dalton Trans.* **2015**, *44*, 7148–7151. [CrossRef] [PubMed]
54. Hu, K.-Q.; Jiang, X.; Wu, S.-Q.; Liu, C.-M.; Cui, A.-L.; Kou, H.-Z. Slow magnetization relaxation in $Ni^{II}Dy^{III}Fe^{III}$ molecular cycles. *Inorg. Chem.* **2015**, *54*, 1206–1208. [CrossRef] [PubMed]
55. Liu, M.-J.; Hu, K.-Q.; Liu, C.-M.; Cui, A.-L.; Kou, H.-Z. Metallocyclic $Ni_4Ln_2M_2$ single-molecule magnets. *Dalton Trans.* **2017**, *46*, 6544–6552. [CrossRef]
56. Dhers, S.; Costes, J.-P.; Guionneau, P.; Paulsen, C.; Vendier, L.; Sutter, J.-P. On the importance of ferromagnetic exchange between transition metals in field-free SMMs: Examples of ring-shaped hetero-trimetallic $[(LnNi_2)\{W(CN)_8\}]_2$ compounds. *Chem. Commun.* **2015**, *51*, 7875–7878. [CrossRef]
57. Ghosh, S.; Mahapatra, P.; Kanetomo, T.; Drew, M.G.B.; Ishida, T.; Ghosh, A. Syntheses, crystal structure and magnetic properties of an unprecedented one-dimensional coordination polymer derived from an $\{(NiL)_2Ln\}$ node and a pyrazine spacer (H_2L = *N*,*N*′-bis(salicylidene)-1,3-propanediamine, Ln = Gd, Tb and Dy). *ChemistrySelect* **2016**, *1*, 2722–2729. [CrossRef]
58. Ion, A.E.; Nica, S.; Madalam, A.M.; Maxim, C.; Julve, M.; Lloret, F.; Andruh, M. One-dimensional coordination polymers constructed from di- and trinuclear {3d-4f} tectons. A new useful spacer in crystal engineering: 1,3-bis(4-pyridyl)azulene. *CrystEngComm* **2014**, *16*, 319–327. [CrossRef]
59. Palacios, M.A.; Morlieras, J.; Herrera, J.M.; Mota, A.J.; Brechin, E.K.; Triki, S.; Colacio, E. Synthetic ability of dinuclear mesocates containing 1,3-bis(diazinecarboxamide)benzene bridging ligands to form complexes of increased nuclearity. Crystal structures, magnetic properties and theoretical studies. *Dalton Trans.* **2017**, *46*, 10469–10483. [CrossRef]
60. Colacio, E.; Palacios, M.A.; Rodríguez-Diéguez, A.; Mota, A.J.; Herrera, J.M.; Choquesillo-Lazarte, D.; Clérac, R. 3d-3d-4f chain complexes constructed using the dinuclear metalacyclic complex $[Ni_2(mbpb)_3]^{2-}$ [H_2mbpb = 1,3-bis(pyridine-2-carboxamide)benzene] as a ligand: Synthesis, structures, and magnetic properties. *Inorg. Chem.* **2010**, *49*, 1826–1833. [CrossRef]
61. Wang, D.; Niu, C.-J.; Li, X.-Z.; Zhu, L.-N.; Hao, P.-P. Syntheses, crystal structures and properties of lanthanide complexes featuring infinite molecular rectangle strands constructed from a new macrocyclic metalloligand. *Inorg. Chim. Acta* **2012**, *391*, 20–27. [CrossRef]

62. He, Z.; He, C.; Gao, E.-Q.; Wang, Z.-M.; Yang, X.-F.; Liao, C.-S.; Yan, C.-H. Lanthanide-transition heterometallic extended structures with novel orthogonal metalloligand as building block. *Inorg. Chem.* **2003**, *42*, 2206–2208. [CrossRef] [PubMed]
63. Li, J.-X.; Guo, W.-B.; Du, Z.-X.; Huang, W.-P. Monometallic nickel and bimetallic nickel-europium complexes based on oxydiacetic acid and N-heterocyclic ligands. *Inorg. Chim. Acta* **2011**, *375*, 290–297. [CrossRef]
64. Liu, F.-C.; Zeng, Y.-F.; Jiao, J.; Li, J.-R.; Bu, X.-H.; Ribas, J.; Batten, S.R. Novel heterometallic 3d-4f metal-azido complex of mixed ligands with unprecedented structure type: Synthesis, structure, and magnetic properties. *Inorg. Chem.* **2006**, *45*, 6129–6131. [CrossRef] [PubMed]
65. Mondal, K.C.; Sengupta, O.; Dutta, P.; Seehra, M.; Nayak, S.K.; Mukherjee, P.S. Three-dimensional 3d-4f heterometallic polymers containing both azide and carboxylate as co-ligands. *Inorg. Chim. Acta* **2009**, *362*, 1913–1917. [CrossRef]